# Design of a Continuous Supersonic Expansion Discharge Source for the Acquisition of a Rotationally-Cold Vibrational Spectrum of $CH_5^+$ with the SCRIBES Instrument

Prospectus for Preliminary Examination

Department of Chemistry, School of Chemical Sciences
University of Illinois
Kyle Crabtree

14 October 2009

A414 CLSL

2:00 PM

## I. INTRODUCTION

The nascent field of astrochemistry seeks to understand the chemical evolution of astronomical entities. In order to answer such questions as the chemical origin of life, efforts to model the reaction networks of various interstellar and circumstellar environments must be guided by astronomical observations of the densities, spatial distributions, and identities of the species present in those regions. The astronomical observations, in turn, can only be accomplished if high-resolution laboratory spectroscopy has been performed on the relevant molecules, radicals, and ions. Considering the low densities and temperatures of most regions of space, gas-phase chemistry is dominated by fast ion-molecule reactions. Consequently, high-resolution spectroscopy of astronomically-important molecular ions is essential for furthering our understanding of the chemistry occurring in the universe around us.

The main challenge with high-resolution spectroscopy of molecular ions in the laboratory has been producing them in sufficient quantities. Positive column glow discharges [1] and negative glow hollow cathode discharges [2, 3] have been used profitably over the past three decades because of the high ion column densities produced. However, even when the walls of these discharge cells are cryogenically cooled, the ion temperatures typically reach only 200-400 K. For larger molecules with more complex spectra, such high temperatures are undesirable because of spectral congestion (see Fig. 1) or spectral intensity dilution, and so other ionization techniques are needed.

In order to produce cold gas-phase ions for spectroscopy, many groups have coupled an electrical discharge with a supersonically-expanding jet of gas seeded with appropriate precursor molecules. The adiabatic expansion of the gas results in rapid cooling, allowing the ions and radicals generated within the discharge plasma to achieve temperatures below 30 K [6]. The majority of these "supersonic expansion discharge sources" are pulsed, operating at a low duty cycle in order to maintain a suitable vacuum [7, 8]. In order to achieve the highest possible sensitivity from a spectroscopic technique, it is desirable to maximize the technique's duty cycle. The SCRIBES (Sensitive, Cooled, Resolved Ion BEam Spectroscopy) experiment being developed in the McCall laboratory (see Fig. 2) requires a continuous source of rotationally-cold ions for ultrasensitive spectroscopy. While continuous "corona-excited" supersonic expansion discharge sources have been developed in the past [9], they are inadequate for SCRIBES because, in addition to problems with nozzle clogging and

deformation, the requirement for a downstream electrode complicates the extraction of an ion beam from the expanding plasma. Therefore, to enable spectroscopy of complex ions at low temperatures with SCRIBES a new ion source must be developed.

## II. PROGRESS

### A. Design of a Continuous Supersonic Expansion Discharge Source

The SCRIBES experiment demands high performance from an ion source. As such, two goals I set for the design of the continuous supersonic expansion source were durability and modularity. In order to obtain high-resolution spectra, the source performance (both the rotational cooling offered by the source as well as the ion density produced) must remain essentially constant over long periods of operation, necessitating a robust and durable source. Also, in the event that a source fails or its performance needs to be tuned, the ability to rapidly exchange/replace individual source components in a modular fashion becomes invaluable for minimizing instrument downtime. Keeping these goals in mind, I have designed and constructed a prototype continuous supersonic expansion discharge source for use with the SCRIBES experiment (see Fig. 3).

In an effort to achieve high durability, I chose to base the source design on materials that could withstand the heat load generated by a continuously-running plasma. The electrodes in the prototype are constructed of stainless steel and the insulator pieces are constructed of Macor, a nonporous machinable ceramic that can withstand high temperatures with low thermal expansion (maximum continuous operating temperature: 800 ℃) [10]. However, requiring the source to be modular complicates the design process, preventing the components from being held together by soldering or brazing. Instead, the parts are secured by six screws which compress the source axially and align the gas channel. To maintain leak-tight seals a high-temperature silicone o-ring is placed at each component interface. The result is a source consisting of a baseplate (anode), a spacer, an electrode (cathode), and a cap, any of which can be easily replaced or exchanged without affecting the other pieces.

Within this base design, a wide parameter space is available for optimizing the source performance in terms of rotational temperature and ion number density. In addition to the traditional parameters used in supersonic expansion sources, such as gas pressure/composition

and discharge current, the geometry of the various source components can be easily varied. The diameters and lengths of the baseplate, spacer and cap can be independently adjusted. Also, by modifying the cap and electrode as a pair, the nozzle geometry can be changed (i.e. pinhole vs. Pierce vs. trumpet flare vs. Laval). With such a wide range of permutations on the base design it is important to test the source independently of the SCRIBES instrument in order to understand its properties in isolation.

### B. Stress-Testing of Supersonic Source

As an initial metric of source performance, I subjected various prototype sources to stress tests in which they were run continuously for long periods of time under simulated operating conditions. After a few minor design revisions from earlier source versions not mentioned here, the prototype source was able to operate for 125 hours under conditions of 1-2 atm $N_2$ gas with an applied voltage of -500 V at a current of 14 mA (see Fig. 4). Even after this extended use, the source still seemed to be fully operational. While this test is a good indicator of the overall source durability, it does not at all assess how well the source actually performs over long periods of time; only that the materials themselves do not degrade over time.

### C. Construction of a Mid-IR "Continuous-Wave" Cavity Ringdown Spectrometer to Assess Source Performance

A better method for characterizing source performance is to spectroscopically monitor the temperatures and densities of ions produced by the source over time. As an initial target for this type of testing, I chose to look at the $\nu_2$ fundamental vibrational band of $H_3^+$ at 3.67 $\mu$m. Our group has previously studied this band in a pulsed supersonic expansion source using "continuous-wave" cavity ringdown spectroscopy [11], observing rotational temperatures around 80 K. Unfortunately, the spectrometer used in those studies was no longer available, and so a new spectrometer had to be built for this purpose. To do so, I had to add a new vacuum chamber to our pumpline, and acquire a new optics table and new lasers.

With help from several other students, I modified the 12 in. diameter PVC vacuum line attached to our 2000 $m^3$/h Roots blower system in order to include an additional vacuum

chamber specifically for testing supersonic expansion sources. After this modification, we observed severe vibrations coupling into our vacuum chambers (and, therefore, ringdown cavities) from the pumping system. To address this problem, I consulted with a mechanical engineer who aided me in designing a vibration damping system for the pumping system, pictured in Fig. 5. Construction of this system greatly reduced the chamber and cavity vibrations, providing a more stable environment for cavity ringdown spectroscopy.

To produce light at 3.67 $\mu$m, I constructed a difference frequency generation laser (DFG) similar to that described in [12], which I had helped to build. In this system, the 10 W, 532 nm output of a frequency-doubled Nd:$YVO_4$ laser is split into two beams. One beam ($\sim$7.5 W) is used to pump a ring dye laser operating at 623 nm (dye: Rhodamine 640 perchlorate). The other beam ($\sim$2.5 W) is sent through an acousto-optic modulator (AOM). The first-order beam is passed through a series of lenses to adjust its focal properties to match those of the dye laser beam. The 532 and 623 nm beams are combined on a dichroic window, made collinear and focused into a MgO-doped periodically-poled lithium niobate crystal. Nonlinear mixing is achieved via quasi-phase matching, and 500-700 $\mu$W of 3.67 $\mu$m laser light is produced. By tuning the dye laser, the DFG can be tuned from 2.2-4.8 $\mu$m.

The "continuous-wave" cavity ringdown technique has been employed frequently by our research group to perform high-resolution spectroscopy of molecules and ions [11–14]. For this spectrometer, an optical cavity is formed by two highly-reflective mirrors [R (3600 nm) $\geq$ 0.9998], and its resonant frequency is adjusted by dithering a piezoelectric transducer attached to one of the mirrors. Light from the DFG is coupled into the cavity. When the cavity resonance frequency matches the laser frequency, light rapidly builds up inside the cavity. The light intensity leaking from the rear mirror is monitored with a liquid-nitrogen-cooled InSb detector. When the intensity reaches a predetermined threshold, the AOM is turned off, effectively switching off the DFG. The light in the cavity exponentially decays; the decay trace is digitized and its time constant $\tau$ determined. Because $\tau$ is related to the cavity losses, when an absorption feature is present at the resonant wavelength, a decrease in $\tau$ is observed. A spectrum is recorded by step-scanning the DFG through frequency space, and recording $\tau$ at each point.

### D. Spectroscopy of $H_3^+$ ($\nu_2 \leftarrow 0$) as a Temperature Probe of Ions Produced in the Supersonic Expansion Discharge Source

$H_3^+$ is the dominant ionic species in a hydrogenic plasma [15], and it is formed by the reaction $H_2^+ + H_2 \rightarrow H_3^+ + H$ [16]. It exists in two nuclear spin modifications, *ortho* ($I = 3/2$) and *para* ($I = 1/2$). In the vibrational ground state, due to symmetry, states with $K = 3n$ are only allowed in *o*-$H_3^+$, and states with $K = 3n \pm 1$ are only allowed in *p*-$H_3^+$. The $(J, K) = (0, 0)$ state is forbidden by the Pauli exclusion principle, so the three lowest-energy states are the (1,1), (1,0), and (2,2) states, with energies of 64.12, 86.96, and 169.29 $cm^{-1}$, respectively. From these states, three fundamental rovibrational transitions fall close together in frequency space within the tuning range of the DFG: $R(1,0)$, $R(1,1)^u$, and $R(2,2)^l$ (see Fig. 6). Together, these transitions can be used as a probe of the temperature of $H_3^+$ produced in the plasma.

To generate $H_3^+$, I constructed a source consisting of a 500 $\mu$m diameter baseplate, a 1 mm diameter, 2.5 mm thick spacer, a 1 mm diameter, 12.7 mm thick electrode, and a 1 mm thick cap. The electrode and cap were machined together into a geometry similar to the bell of a trumpet. The source was mounted inside a vacuum chamber, and fed with $H_2$ gas at 2 atm backing pressure. A discharge was struck at -200 V with a current of 25 mA. The source was positioned such that the laser beam intersected the plasma expansion 1 cm downstream of the source.

Spectra of the $R(1,0)$ and $R(1,1)^u$ transitions were acquired initially. A sample spectrum is shown in Fig. 7. Using the formula

$$\frac{n_{(1,0)}}{n_{(1,1)}} = \frac{\mu^2_{R(1,1)^u}}{\mu^2_{R(1,0)}} \frac{I_{R(1,0)}}{I_{R(1,1)^u}} = \frac{g_{I(1,0)}}{g_{I(1,1)}} \exp\left(-\frac{E_{(1,0)} - E_{(1,1)}}{k_B T_{ex}}\right), \tag{1}$$

where $n$ is the number density, $\mu$ is the transition dipole moment, $I$ is the observed intensity, and $g_I$ is the nuclear spin degeneracy, the "excitation temperature" of the $H_3^+$ ions was calculated. For scans with suitably high signal-to-noise ratios, the typical excitation temperatures observed were on the order of 40 $\pm$ 10 K. However, at such low temperatures the ratio of the R(1,0) and $R(1,1)^u$ transition intensities is not a useful indicator of the true rotational temperature. For these scans, it can only be concluded that the true rotational temperature is below 50 K. A more appropriate indicator is the ratio of the $R(1,1)^u$ and $R(2,2)^l$ intensities; efforts are currently underway to make these measurements.

## III. FUTURE DIRECTIONS

### A. Additional Supersonic Expansion Discharge Source Testing

In addition to the spectroscopic stress testing, I plan to conduct more extensive tests on the source design parameter space. Specifically, I would like to test the "exit geometry" of the source. Traditionally, radially-symmetric sources (as opposed to slit-jet sources) have been based on a capillary-like design, in which the gas channel is nothing more than a straight hole drilled through the source body. However, it has been reported [17] that a trumpet-shaped nozzle produces a jet with a greater on-axis number density, and therefore, lower on-axis temperatures as compared to a pinhole source. Such properties would be beneficial to the SCRIBES experiment, so it is worth testing if these properties remain true for the supersonic expansion discharge source.

For these tests, $H_3^+$ is not an ideal target as a temperature probe, owing to its high rotational constants ($B = 43.56$ cm$^{-1}$ and $C = 20.61$ cm$^{-1}$) [18]. Instead, I propose to observe the $\nu_1$ band of $HN_2^+$ at 3.1 $\mu$m using the same cavity ringdown technique used for $H_3^+$. This species has a much lower rotational constant ($B = 1.554$ cm$^{-1}$), and is readily produced in a discharge environment [19]. Xu *et al.* observed this ion with a rotational temperature of 33 K in a corona-slit supersonic expansion discharge source using concentration modulation with multipass infrared absorption spectroscopy [20], and I anticipate that my prototype source will be able to produce similar, if not even lower temperatures.

During the comparison of source performance as a function of nozzle geometry, I will also vary the gas pressure and discharge current in an effort to determine optimal operating conditions for the production and cooling of $HN_2^+$. These conditions will be useful for integrating the supersonic source with SCRIBES (see following section), but will also serve as a basis for comparison with larger, more complex ions.

### B. Integration of the Supersonic Expansion Discharge Source with SCRIBES

In order to integrate the supersonic expansion discharge source with SCRIBES, an ion beam must be extracted from the expanding plasma. Supersonic expansion sources have long been used to produce molecular beams by means of inserting a skimmer into the gas flow, but this approach is more challenging for continuous expansions operating at high

pressures (0.01-1 Torr) [21]. Particularly, formation of detached shocks in the body of the expansion and background gas penetration due to gas reflection from the skimmer wall can cause heating of the expansion core. Nevertheless, it has been shown that careful skimmer design and positioning can eliminate these problems [22].

Skimmers that meet the conditions discussed in [22] are commercially available from Beam Dynamics. It may be advantageous, however, to build skimmers in-house for more rapid testing and easier replacement. Also, because the optimum skimmer geometry depends on the actual conditions of the supersonic expansion, using the source to produce various ions of astrochemical interest will necessitate using a variety of skimmer geometries to deal with the changing source conditions. Jordan *et al.* have described a procedure for machining refractory skimmers from graphite whose performance is comparable to commercial skimmers from Beam Dynamics [23]. I have confirmed with Bill Knight that the SCS Machine Shop is capable of machining these skimmers as specified.

My labmates who are actively working on the SCRIBES instrument have integrated a number of diagnostic measures for assessing the quality of the ion beam itself. The profile of the ion beam can be measured at a variety of locations using commercial beam profile monitors; the beam current can be measured by a number of insertable/removable Faraday cups; and the beam energy, velocity spread, and composition can be measured using a homebuilt beam-modulated time-of-flight mass spectrometer. These diagnostics will aid in the alignment and positioning of the supersonic source with respect to the skimmer.

Once the ion beam has been successfully extracted and optimized, the SCRIBES instrument can undergo its first complete spectroscopic characterization. For this purpose, spectroscopy of the $\nu_1$ band of $HN_2^+$ will again be used to determine the beam's rotational temperature and number density. The results of the spectroscopy will allow us to optimize both the source operating conditions as well as the efficiency of coupling the source to the ion beam.

### C. Acquisition of a Rotationally Cold Rovibrational Spectrum of $CH_5^+$

$CH_5^+$, protonated methane, is the simplest example of a protonated carbocation and is of great interest in astrochemistry and theoretical chemistry. In space, it is involved with the gas-phase chemistry of dense molecular clouds [24], and may also be implicated in

deuterium fractionation via the reaction $CH_3^+ + HD \rightarrow CH_4D^+ \rightarrow CH_2D^+ + H_2$ [25]. $CH_5^+$ may also be responsible for the pathway to the formation of carbon-carbon bonds in the gas phase (see Fig. 8) [18]. From a theoretical standpoint, its intramolecular dynamics involves such large-amplitude motions that even the traditional concept of "molecular structure" has been challenged for this species [26]. Attempts to understand the quantum mechanics and dynamics of this ion continue to this day.

The potential energy surface of $CH_5^+$ consists of 120 equivalent potential minima and it is generally understood that the structure at this point is an $H_2$ subunit on top of a $CH_3^+$ tripod, called the $C_s$(I) structure. However, there are also 180 low-lying saddle points on the surface: 120 correspond to a $C_s$(II) structure located 30-40 $cm^{-1}$ above the global minima, and 60 to a $C_{2v}$ structure located 300-350 $cm^{-1}$ above the minima (see Fig. 9) [27]. The molecule can sample all 120 minima by means of a combination of internal rotations through the $C_s$(II) saddle point and "flip" motions through the $C_{2v}$ saddle point.

Most theoretical studies of the dynamics of $CH_5^+$ have focused on understanding the large-amplitude motion in the space defined by these states. Car-Parinello path-integral studies [28] as well as diffusion Monte Carlo studies [29] have shown that the structure is highly fluxional, and that the ion spends approximately 80% of its time in one of the two $C_s$ structures. As a result, the distribution of H-H distances within the molecule as it samples the potential surface is expected to display a peak around 1.9 Å corresponding to the $CH_3$ tripod, with a shoulder around 1.0 Å corresponding to the $H_2$ moiety. Efforts to calculate the millimeter spectrum that would result from the dynamics have been made; however, no such spectrum has yet been observed [30].

Experimental guidance is available for calculations of the vibrational structure of $CH_5^+$. Recently a low-resolution laser-induced reaction spectrum has been acquired with the free electron laser FELIX [31]. It shows two main features: a broad structure from 2500-3200 $cm^{-1}$ that has been assigned to C-H stretching modes and a narrower feature around 1200 $cm^{-1}$ that has been assigned to H-C-H rocking motions [32]. The calculations employed in the assignment of this spectrum suffered from a shift of around 100 $cm^{-1}$ and the agreement is still rough even after taking this shift into account. In spite of even this agreement, some features predicted in the calculations are not observed in the experimental spectrum.

The minor success with interpreting the FELIX spectrum notwithstanding, the true challenge for $CH_5^+$ is to understand the high-resolution spectrum from 2800-3100 $cm^{-1}$ acquired

by Oka and coworkers [4, 5]. Several approaches have been utilized to calculate vibrational energy levels and the spectrum of $CH_5^+$. Bunker and coworkers attempted to use coordinates based on the internal rotation and flip pathways discussed earlier to reduce the dimensionality of the calculation [30], and Nesbitt and coworkers attempted to do the same with a "particle-on-a-sphere" model [33, 34]. Full-dimensional normal-mode calculations were attempted by Bowman and coworkers [32], but none of these approaches has provided any hints at an interpretation of the spectrum.

One promising approach is described by Wang and Carrington: using basis set contraction methods along with the Lanczos algorithm, they have been able to perform full-dimensional variational calculations without the need for a reference geometry (as is done for a normal-mode calculation) [35]. While they have not yet attempted to include rotations into their calculations, their approach should provide energy levels suitable for interpreting the spectrum. Most interestingly, they show that the pattern of vibrational energy levels does not depend on the structure at the bottom of the potential energy surface or on the curvature of the minima (i.e., the harmonic frequencies).

However, the ultimate answer to solving this problem will be the acquisition of a rotationally cold spectrum. The spectrum acquired by Oka suffers not only from congestion, but also from complications arising from the high temperature. Because no known model exists for predicting the structure or patterns present in the spectrum, it is impossible to know which lines might correspond to low-$J$ or high-$J$ levels. By comparing a rotationally cold spectrum to the warm spectrum, it will be possible to determine the band origin and energy spacings, and this is the first step in unraveling the spectrum.

Experimentally, $CH_5^+$ can be produced effectively in a $CH_4$ or $CH_4/H_2$ plasma by the fast Langevin rate ($\sim 1\times10^{-9}$ cm$^{-3}$ sec$^{-1}$) reactions:

$$CH_4^+ + CH_4 \rightarrow CH_5^+ + CH_3 \tag{2}$$

$$CH_4 + H_3^+ \rightarrow CH_5^+ + H_2 \tag{3}$$

Under these conditions, $CH_5^+$ is primarily destroyed by dissociative recombination with electrons, as its proton affinity is higher than that of either $CH_4$ or $H_2$ [4]. Production in a supersonic expansion environment should be easily achieved by using about a 10:1 mixture of $H_2/CH_4$ seeded in an inert buffer gas, such as Ar or He. An advantage of the SCRIBES

instrument is the inclusion of a mass spectrometer, which will allow for adjusting the gas composition, pressure, and discharge current to optimize production of $CH_5^+$ by peaking the signal at $m/z = 17$.

The spectroscopic technique employed will be beam-velocity-modulated cavity-enhanced absorption spectroscopy (BVM-CEAS). In this technique, a laser is locked to a high-finesse optical cavity that surrounds the ion beam formed in the SCRIBES instrument. A conductive tube is placed around the ion beam in the drift region, and a square wave voltage is applied to slightly modulate the velocity of the ions. The cavity output is then demodulated to reveal the absorption spectrum as the laser is scanned. The sensitivity of this technique is the same as traditional velocity-modulation absorption spectroscopy, but the effective absorption pathlength is increased greatly by cavity-enhancement ($\sim$5000 m for a 1 m cavity with 99.98 % reflective mirrors). Additionally, the rotational cooling offered by the expansion will increase the intensity for low-lying rotational levels, and the kinematic compression effect will decrease the transition linewidths.

Compared with the experimental conditions of Oka's spectrometer [4], $CH_5^+$ should be observable with SCRIBES/BVM-CEAS. A rough estimate of the expected number density inside the drift region, based on the fractional transmission of a skimmer acting on a supersonic expansion [21], is $10^7$ cm$^{-3}$. Although the $CH_5^+$ number density in Oka's discharge cell was $10^{10}$ cm$^{-3}$, our effective absorption path length is 3 orders of magnitude larger (5000 m vs. 6 m). Moreover, with an expected rotational temperature of $\sim$20 K, the populations of the $J = 0, 1$ levels should be higher by about an order of magnitude compared to theirs at $\sim$300 K, and our linewidths should be about 20 MHz due to kinematic compression, instead of their Doppler-broadened 300 MHz. Therefore, I expect that we should have no trouble observing this ion with SCRIBES.

## IV. CONCLUSIONS

I have developed and begun initial characterization of a prototype continuous supersonic expansion discharge source. The design of the source is modular and robust, and is capable of producing rotationally cold molecular ions in quantities sufficient for spectroscopy. After performing additional characterization of the source and integrating it with the SCRIBES instrument, I propose to acquire a rotationally cold spectrum of $CH_5^+$ using beam-velocity-

modulated cavity-enhanced absorption spectroscopy. The cooling offered by the source as well as the unique advantages of the SCRIBES instrument should allow me to obtain a spectrum which will further the understanding of the intramolecular dynamics of this species, which has intrigued scientists for decades.

---


[1] R. C. Woods, "A microwave spectrometer with an internal glow discharge" *Rev. Sci. Instrum.* (1973), **44**, 282–288.

[2] C. M. Gabrys, D. Uy, M.-F. Jagod, T. Oka, T. Amano, "Infrared spectroscopy of carboions. 8. Hollow cathode spectroscopy of protonated acetylene, $C_2H_3^+$" *J. Phys. Chem.* (1995), **99**(42), 15611–15623.

[3] T. Amano, "High-resolution infrared spectroscopy of molecular ions" *Phil. Trans. R. Soc. London Ser. A* (1988), **324**(1578), 163–178.

[4] E. T. White, "High resolution laser spectroscopy of $CH_5^+$" Ph.D. thesis, University of Chicago (1999).

[5] E. T. White, J. Tang, T. Oka, "$CH_5^+$: The infrared spectrum observed" *Science* (1999), **284**(5411), 135–137.

[6] D. T. Anderson, S. Davis, T. S. Zwier, D. J. Nesbitt, "An intense slit discharge source of jet-cooled molecular ions and radicals ($T_{rot} < 30$ K)" *Chem. Phys. Lett.* (1996), **258**(1-2), 207–212.

[7] M. C. McCarthy, W. Chen, M. J. Travers, P. Thaddeus, "Microwave spectra of 11 polyyne carbon chains" *Astrophys. J. Suppl. Ser.* (2000), **129**, 611–623.

[8] L. Biennier, F. Salama, L. J. Allamandola, J. J. Scherer, "Pulsed discharge nozzle cavity ringdown spectroscopy of cold polycyclic aromatic hydrocarbon ions" *J. Chem. Phys.* (2003), **118**(17), 7863–7872.

[9] P. C. Engelking, "Corona excited supersonic expansion" *Rev. Sci. Instrum.* (1986), **57**(9), 2274–2277.

[10] "Macor specifications" http://www.corning.com/docs/specialtymaterials/pisheets/Macor.pdf.

[11] B. A. Tom, "Nuclear spin dependence in reactions of $H_3^+$ in the laboratory and the interstellar medium" Ph.D. thesis, University of Illinois (2009).

[12] A. A. Mills, "Construction of the SCRIBES (Sensitive Cooled Resolved Ion BEam Spec-

troscopy) instrument for the detection of astrochemically important molecular ions" Research Prospectus for Preliminary Examination (2007).

[13] B. E. Brumfield, "High-resolution spectroscopic studies of $C_{60}$ and $C_6H_7^+$: Molecules of fundamental spectroscopic and astrochemical importance" Research Prospectus for Preliminary Examination (2007).

[14] S. L. Widicus Weaver, M. B. Wiczer, B. Negru, J. P. DiGangi, B. A. Tom, B. J. McCall, "Continuous-wave cavity ringdown spectroscopy of the Meinel system (2, 1) band" *J. Mol. Spectrosc.* (2008), **249**(1), 14–22.

[15] A. J. Dempster, "The ionization and dissociation of hydrogen molecules and the formation of $H_3$" *Phil. Mag.* (1916), **31**, 438–443.

[16] T. R. Hogness, E. G. Lunn, "The ionization of hydrogen by electron impact as interpreted by positive ray analysis" *Phys. Rev.* (1925), **26**(1), 44–55.

[17] U. Even, "Recent advances in pulsed supersonic sources" in "63$^{\rm rd}$ OSU International Symposium on Molecular Spectroscopy", (2008) .

[18] B. J. McCall, "Spectroscopy of $H_3^+$ in laboratory and astrophysical plasmas" Ph.D. thesis, University of Chicago (2001).

[19] C. S. Gudeman, M. H. Begemann, J. Pfaff, R. J. Saykally, "Velocity-modulated infrared laser spectroscopy of molecular ions: The $\nu_1$ band of $HNN^+$" *J. Chem. Phys.* (1983), **78**(9), 5837–5838.

[20] Y. Xu, M. Fukushima, T. Amano, A. R. W. McKellar, "Infrared absorption spectroscopy of molecular ions in a corona-discharge slit expansion" *Chem. Phys. Lett.* (1995), **242**(1-2), 126–131.

[21] R. Campargue, "Progress in overexpanded supersonic jets and skimmed molecular beams in free-jet zones of silence" *J. Phys. Chem.* (1984), **88**(20), 4466–4474.

[22] H. C. W. Beijerinck, R. J. F. Van Gerwen, E. R. T. Kerstel, J. F. M. Martens, E. J. W. Van Vliembergen, M. R. T. Smits, G. H. Kaashoek, "Campargue-type supersonic beam sources: Absolute intensities, skimmer transmission and scaling laws for mono-atomic gases He, Ne and Ar" *Chem. Phys.* (1985), **96**(1), 153–173.

[23] D. C. Jordan, R. Barling, R. B. Doak, "Refractory graphite skimmers for supersonic free-jet, supersonic arc-jet, and plasma discharge applications" *Rev. Sci. Instrum.* (1999), **70**(3), 1640–1648.

[24] E. Herbst, "Chemistry of star-forming regions" *J.Phys. Chem. A* (2005), **109**(18), 4017–4029.

[25] H. Roberts, E. Herbst, T. J. Millar, "The importance of new rate coefficients for deuterium fractionation reactions in interstellar chemistry" *Mon. Not. R. Astron. Soc.* (2002), **336**(1), 283–290.

[26] P. Schreiner, "Does $CH_5^+$ have (a) 'structure?' - a tough test for experiment and theory" *Angew. Chem. Int. Ed.* (2000), **39**(18), 3239–3241.

[27] Z. Jin, B. Braams, J. Bowman, "An ab initio based global potential energy surface describing $CH_5^+ \rightarrow CH_3^+ + H_2$" *J. Phys. Chem. A* (2006), **110**(4), 1569–1574.

[28] D. Marx, M. Parrinello, "Structural quantum effects and three-centre two-electron bonding in $CH_5^+$" *Nature* (1995), **375**(6528), 216–218.

[29] A. Brown, A. McCoy, B. Braams, Z. Jin, J. Bowman, "Quantum and classical studies of vibrational motion of $CH_5^+$ on a global potential energy surface obtained from a novel ab initio direct dynamics approach" *J. Chem. Phys.* (2004), **121**(9), 4105–4116.

[30] P. Bunker, B. Ostojic, S. Yurchenko, "A theoretical study of the millimeterwave spectrum of $CH_5^+$" *J. Mol. Struct.* (2004), **695**(Sp. Iss. SI), 253–261.

[31] O. Asvany, P. K. P, B. Redlich, I. Hegemann, S. Schlemmer, D. Marx, "Understanding the infrared spectrum of bare $CH_5^+$" *Science* (2005), **309**(5738), 1219–1222.

[32] X. Huang, A. B. McCoy, J. M. Bowman, L. M. Johnson, C. Savage, F. Dong, D. J. Nesbitt, "Quantum deconstruction of the infrared spectrum of $CH_5^+$" *Science* (2006), **311**(5757), 60–63.

[33] M. Deskevich, D. Nesbitt, "Large amplitude quantum mechanics in polyatomic hydrides. I. A particles-on-a-sphere model for $XH_n$" *J. Chem. Phys.* (2005), **123**(8), 084304.

[34] M. P. Deskevich, A. B. Mccoy, J. M. Hutson, D. J. Nesbitt, "Large-amplitude quantum mechanics in polyatomic hydrides. II. A particle-on-a-sphere model for $XH_n$ $(n = 4, 5)$" *J. Chem. Phys.* (2008), **128**(9), 094306.

[35] X.-G. Wang, J. Tucker Carrington, "Vibrational energy levels of $CH_5^+$" *J. Chem. Phys.* (2008), **129**(23), 234102.

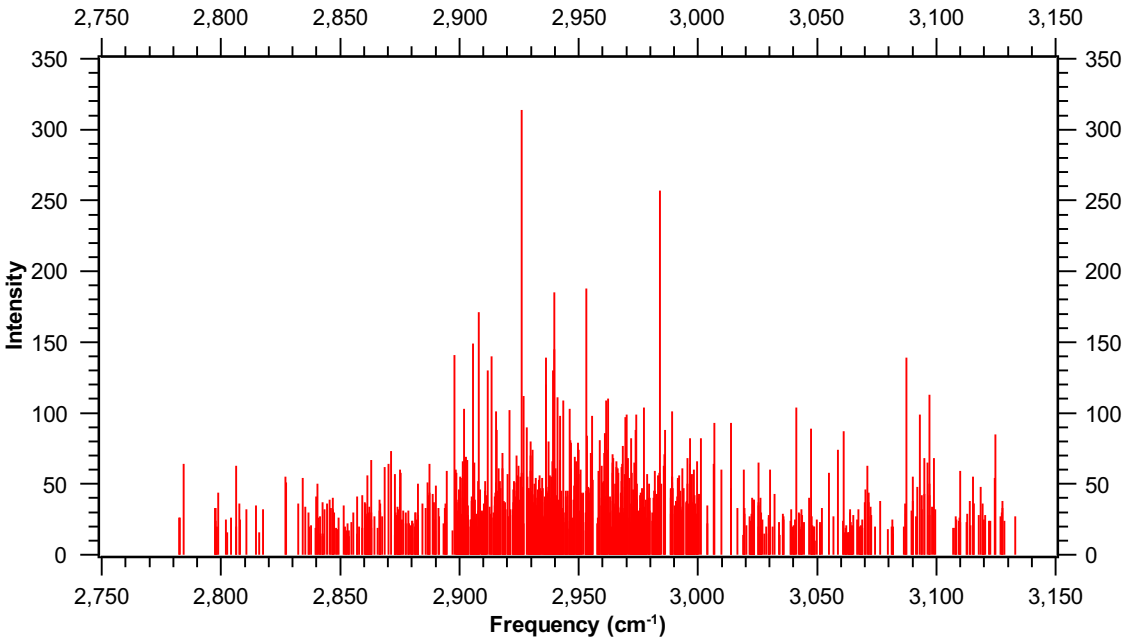


FIG. 1: The vibrational spectrum of $CH_5^+$ recorded in a positive column dc discharge cell at 300-400 K. To date, the spectrum is unassigned because of spectral complexity and congestion. [4, 5]

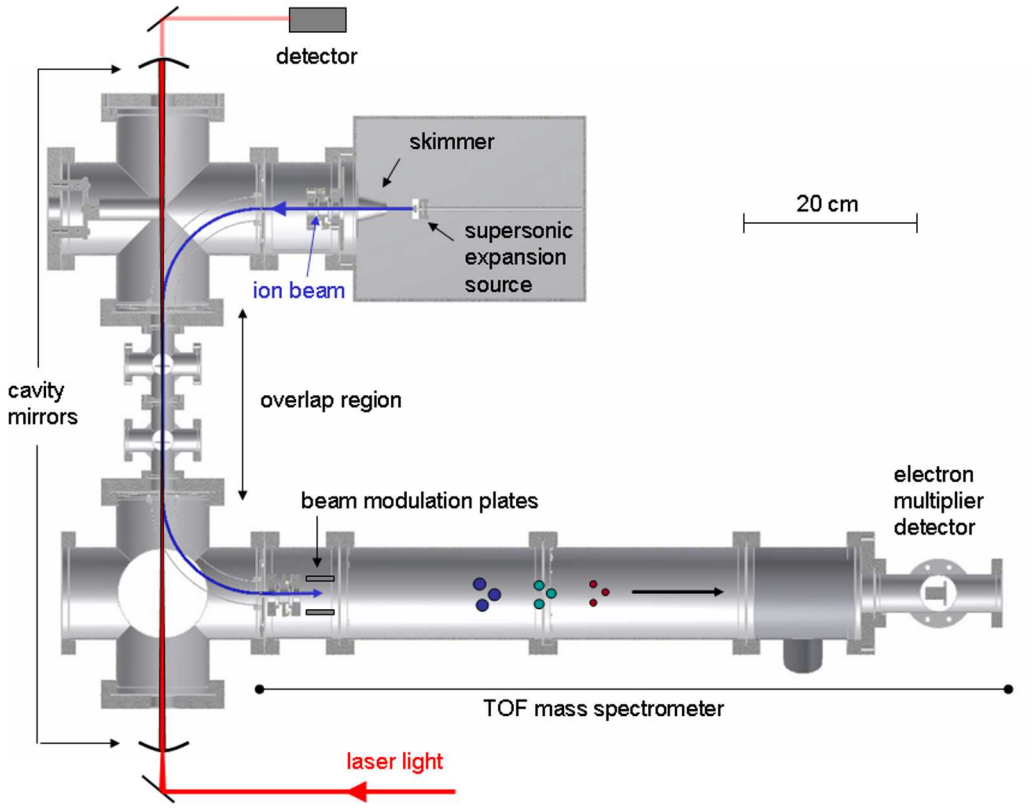


FIG. 2: Diagram of the SCRIBES instrument. Ions are produced and cooled in a supersonically expanding plasma. An ion beam is then extracted by a skimmer, accelerated by ion optics, and steered away from neutral molecules into a field-free drift region, where cavity-enhanced laser spectroscopy is performed. The ions are then steered into a beam-modulated time-of-flight mass spectrometer for mass identification and beam energy analysis.

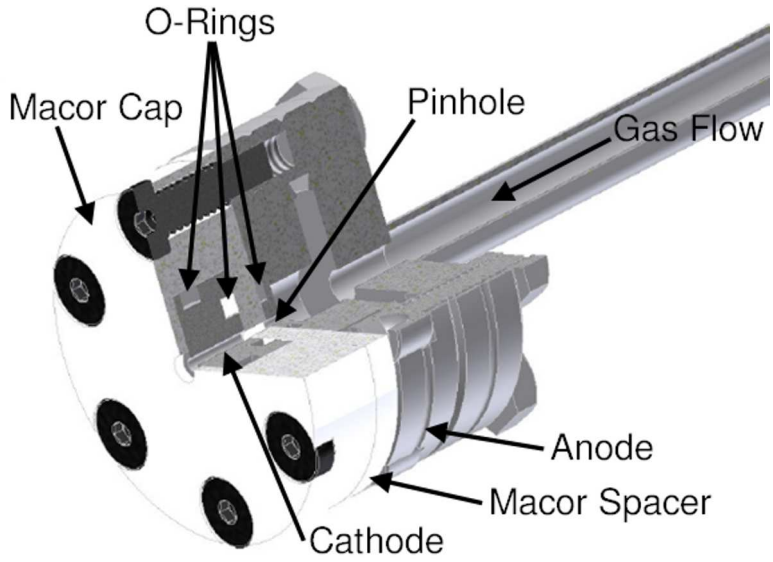


FIG. 3: A cutaway view of the prototype supersonic expansion discharge source. The source is based on a commercial 1.33 in. stainless steel Conflat flange pair that serves as the anode of the electrical discharge and as the pinhole for the expansion source. The anode is separated from the stainless steel cathode by a Macor spacer, and the cathode is encapsulated by another Macor piece. The cathode/Macor assembly is held together by six screws, which provide compression for three o-rings to maintain leak-tightness. Voltage is applied to the cathode by a screw (not pictured) that threads into the electrode through a channel drilled into the cap.

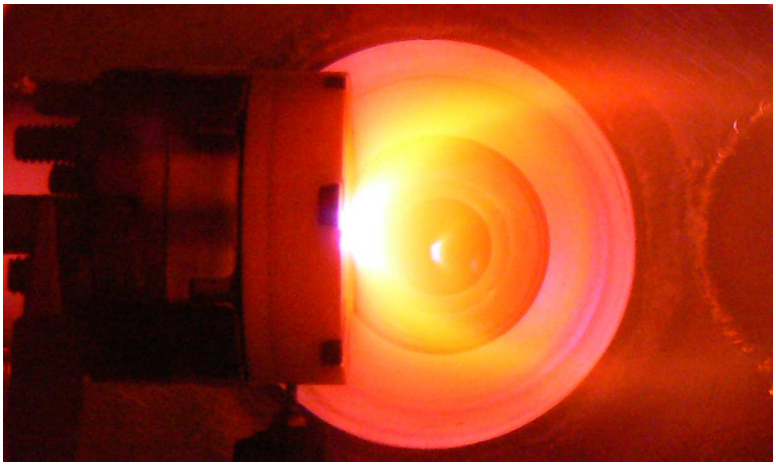

FIG. 4: A photo of the prototype source in operation. The geometry of this source was based on a 500 $\mu$m pinhole. The gas, $N_2$, was discharged at a potential of -500 V with a current of 14 mA.

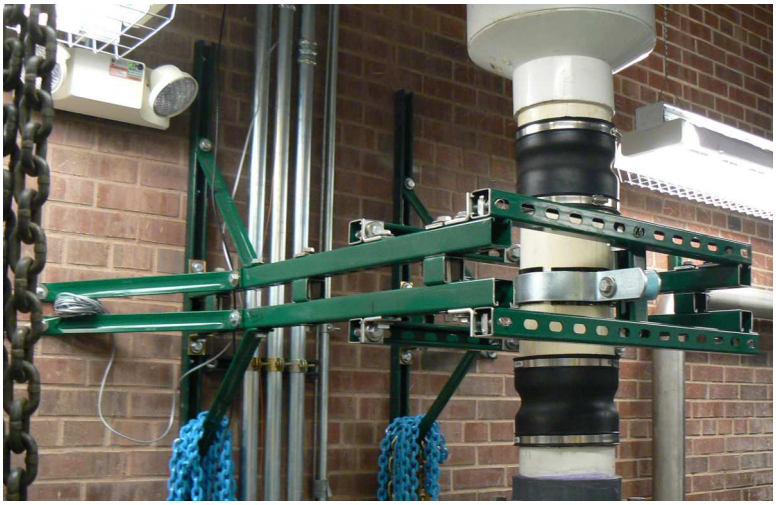

FIG. 5: The vibration-damping system on our 2000 $m^3$/h Roots blower. A section of 6 in. PVC pipe is suspended between two rubber couplers. A riser clamp is attached to the pipe (with rubber), and is attached to a support structure rigidly coupled to the wall. All bolts are fastened with rubber washers for additional vibration damping. The support structure minimizes displacement of the pipe section, which reduces the amount of vibration coupled into the pumpline through the upper rubber coupler.

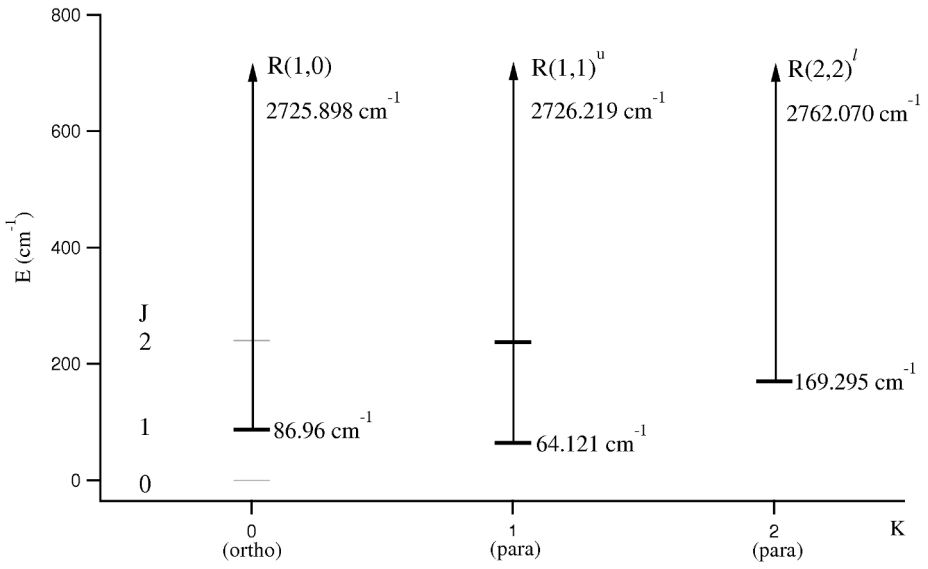


FIG. 6: Ground state energy levels of $H_3^+$ and transitions of interest. Adapted from [11].

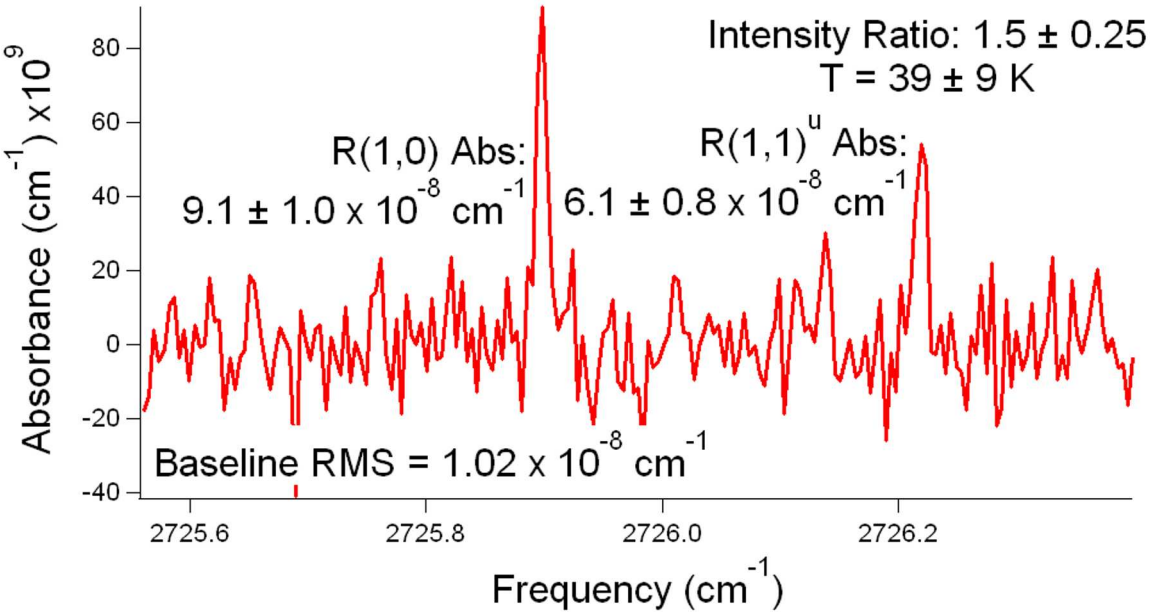


FIG. 7: A sample scan of the R(1,0) and R(1,1)$^u$ lines of $H_3^+$ after baseline subtraction. The temperature was calculated by eq. 1.

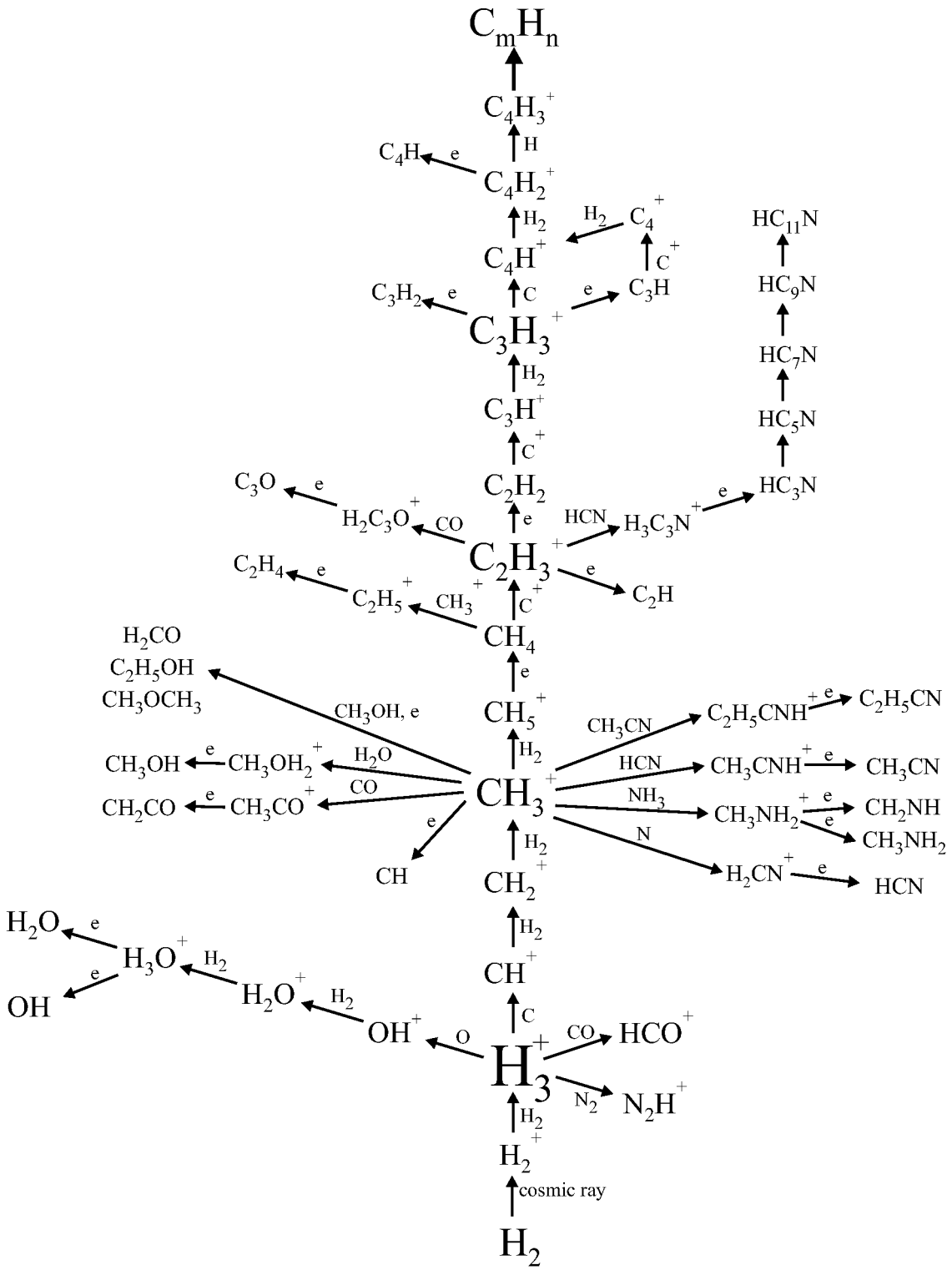


FIG. 8: A proposed network of gas-phase reactions occurring in the interstellar medium. Reproduced from [18].

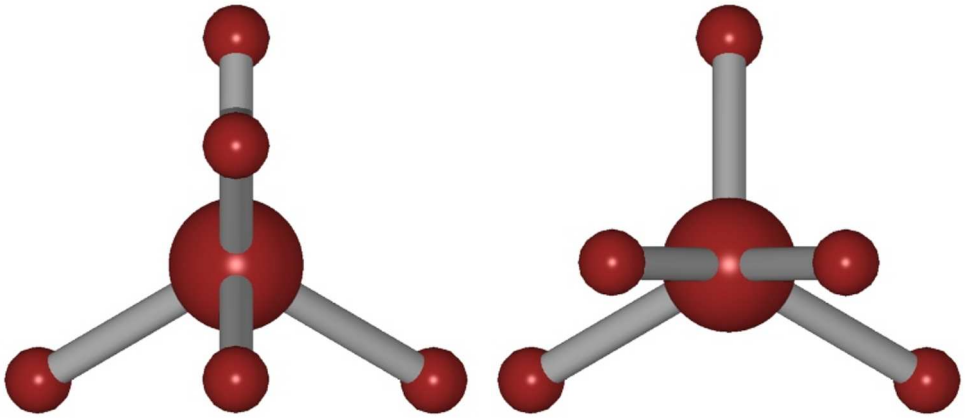

(a)$C_s$(I) structure (b)$C_s$(II) structure

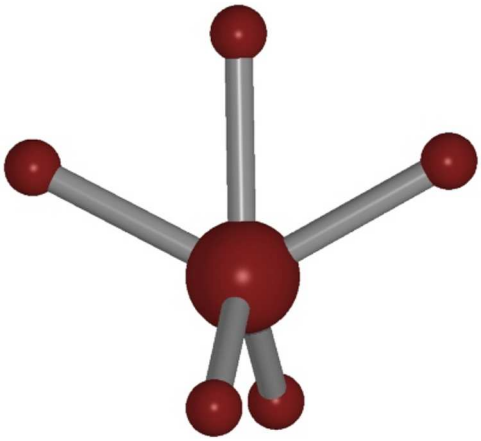

(c)$C_{2v}$ structure

FIG. 9: The three lowest-energy structures of $CH_5^+$. Figures obtained from Takeshi Oka at http://fermi.uchicago.edu.

## Appendix A: Paper Reprints and Preprints

1. Reprint: "Dissociative recombination of highly enriched *para*-$H_3^+$" Journal of Chemical Physics (2009), **130**, 031101.

2. Preprint: "Development and characterization of a source of rotationally cold, enriched *para*-$H_3^+$"

# Dissociative recombination of highly enriched para-$H_3^+$

Brian A. Tom,[1] Vitali Zhaunerchyk,[2] Michael B. Wiczer,[1,a)] Andrew A. Mills,[1] Kyle N. Crabtree,[1] Magdalena Kaminska,[2,3] Wolf D. Geppert,[2] Mathias Hamberg,[2] Magnus af Ugglas,[2] Erik Vigren,[2] Wim J. van der Zande,[4] Mats Larsson,[2] Richard D. Thomas,[2] and Benjamin J. McCall[1,5,b)]

[1]*Department of Chemistry, University of Illinois at Urbana-Champaign, Urbana, Illinois 61801, USA*
[2]*Department of Physics, Stockholm University, Alba Nova, S-106 91 Stockholm, Sweden*
[3]*Institute of Physics, Jan Kochanowski University, Swietokrzyska 15, PL-25406 Kielce, Poland*
[4]*Department of Physics, Radboud University, NL-6500 GL Nijmegen, The Netherlands*
[5]*Department of Astronomy, University of Illinois at Urbana-Champaign, Urbana, Illinois 61801, USA*

(Received 11 September 2008; accepted 15 December 2008; published online 16 January 2009)

The determination of the dissociative recombination rate coefficient of $H_3^+$ has had a turbulent history, but both experiment and theory have recently converged to a common value. Despite this convergence, it has not been clear if there should be a difference between the rate coefficients for ortho-$H_3^+$ and para-$H_3^+$. A difference has been predicted theoretically and could conceivably impact the ortho:para ratio of $H_3^+$ in the diffuse interstellar medium, where $H_3^+$ has been widely observed. We present the results of an experiment at the CRYRING ion storage ring in which we investigated the dissociative recombination of highly enriched ($\sim$83.6%) para-$H_3^+$ using a supersonic expansion source that produced ions with $T_{rot} \sim 60-100$ K. We observed an increase in the low energy recombination rate coefficient of the enriched para-$H_3^+$ by a factor of $\sim$1.25 in comparison to $H_3^+$ produced from normal $H_2$ (ortho:para=3:1). The ratio of the rate coefficients of pure para-$H_3^+$ to that of pure ortho-$H_3^+$ is inferred to be $\sim$2 at low collision energies; the corresponding ratio of the thermal rate coefficients is $\sim$1.5 at electron temperatures from 60 to 1000 K. We conclude that this difference is unlikely to have an impact on the interstellar ortho:para ratio of $H_3^+$. © *2009 American Institute of Physics*. [DOI: 10.1063/1.3065970]

$H_3^+$, the simplest polyatomic molecule, plays a central role in the chemistry of the interstellar medium because it easily protonates most atoms and molecules.[1,2] Consequently, understanding the formation and destruction pathways for this molecular ion under astrophysical conditions is of great importance. Dissociative recombination (DR), the recombination of molecular ions with electrons that leads to dissociation into neutral fragments, is the primary mechanism by which $H_3^+$ is destroyed in diffuse interstellar clouds.[3] The search for the $H_3^+$ DR rate coefficient has had a somewhat turbulent history, with values that varied by orders of magnitude.[4,5] The measurement of rotationally cold $H_3^+$ at CRYRING in 2002,[6] together with complete dimensionality quantum mechanical calculations,[7] has finally brought some level of closure to the debate. In fact, the CRYRING data were recently used to observationally determine the cosmic ray ionization rate in diffuse clouds.[8] Theory[7] also predicted that ground-state ortho-$H_3^+$ recombines faster than the ground state of para-$H_3^+$ at low collision energies. To probe this difference, Kreckel *et al.*[9] studied $H_3^+$ produced from both normal and highly enriched para-$H_2$, and found that para-$H_3^+$ had a higher DR rate coefficient (although the exact ortho:para ratio of $H_3^+$ in their source is unknown). A subsequent theoretical refinement[10] was consistent with this observation. Unfortunately, recent experiments performed at TSR have not been able to replicate this difference.[11] Confirming and characterizing the difference in the DR rate coefficients of ortho- and para-$H_3^+$ are of great importance, not only because of the impact such knowledge can have on our ability to more precisely model astrophysical processes but also because of the basic physical insight we can gain regarding this simple yet pivotal molecular ion.

In the present experiment, the DR of highly enriched para-$H_3^+$ was studied at the CRYRING ion storage ring using a pulsed supersonic expansion ion source. This approach was motivated by the spin selection rules derived by Quack[12] and Oka,[13] which imply that para-$H_2^+$ reacting with para-$H_2$ can only form para-$H_3^+$. We sought to enrich the fraction of para-$H_3^+$ as much as possible and furthermore to precisely measure this fraction in order to characterize the rate coefficient difference between ortho- and para-$H_3^+$.

An enriched >99.9% para-$H_2$ gas was produced using a modified closed-cycle $^4$He cryostat. The enrichment of the para-$H_2$ gas was measured using thermal conductivity[14,15] and NMR. The gas was shipped to the experimental facility at the Manne Siegbahn Laboratory at Stockholm University in a Teflon-lined sample vessel. Tests indicated that the highly enriched para-$H_2$ gas stored in this vessel converted back to ortho-$H_2$ at a rate of $\sim$1.7% per week. Therefore, the gas was $\geq$97% enriched in para-$H_2$ at the time of the experimental runs.

a)Present address: Department of Physics, Massachusetts Institute of Technology, Cambridge, MA 02139.
b)Electronic mail: bjmccall@illinois.edu.

 

The design and operation of the source have been covered in detail elsewhere.[6] In short, the gas emerging from the source pinhole underwent collisional cooling in a supersonic expansion, and was ionized when passing an electrode held at approximately −350 V. About 1500 Torr of backing pressure was used to feed the source, which was pulsed for 400–800 $\mu$s. The source was spectroscopically characterized at the University of Illinois before and after the experiment at CRYRING. This was done in order to verify that our test gas and source conditions produced a plasma that was highly enriched in para-$H_3^+$, and at rotationally cold temperatures. We used continuous-wave (CW) cavity ring-down spectroscopy with a difference frequency laser to probe the ortho-$H_3^+$ $R(1,0)$ and the para-$H_3^+$ $R(1,1)^u$ ground-state rovibrational transitions near 3.67 $\mu$m. Details regarding the difference frequency laser, the integration of the pulsed source with CW ring-down, as well as the source characterization itself will be presented elsewhere. The measured fraction of para-$H_3^+$ was ~49.1% for normal $H_2$ and ~74.7% for 97% para-$H_2$ enriched samples. Because we were seeking the highest fraction of para-$H_3^+$ possible, we experimented with dilutions in argon to reduce the number of $H_3^+ + H_2$ collisions, thereby reducing back-conversion from para- to ortho-$H_3^+$ in the plasma (see Ref. 16). We obtained the highest enrichment using a 1% dilution of para-enriched hydrogen in argon (by pressure), with a para-$H_3^+$ fraction of ~83.6%. The rotational temperature of the ions was measured to be ~60–100 K for all enrichments and dilutions.

Details regarding the experimental method at CRYRING are thoroughly discussed in Ref. 6 but a brief description is provided here for continuity. After exiting the source, the $H_3^+$ ions were mass selected, focused through ion optics floated at 30 kV, accelerated to 900 keV using a radio frequency quadrupole, and finally injected into the ring and accelerated to 13 MeV. The ions, having been rotationally cooled in the expansion, were stored in the ring for up to 5.6 s to allow vibrational relaxation to occur. During this relaxation period, the ions periodically passed through an electron cooler where they interacted with electrons at velocity matching conditions, leading to the translational cooling of the ions. As such, the electron cooler served the dual purpose of reducing the energy distribution of the ions, as well as providing a location where the DR could occur. The electron cooler cathode voltage was linearly ramped from 2965 to 1892 V over a 1 s interval, which covered the interaction energy range from ~0 to ~30 eV. The neutral DR products, no longer subject to the magnetic forces of the ring's bending magnets, emerged tangentially from the ring and were counted by an ion-implanted silicon detector. Measurements were taken such that the rate coefficient, $\alpha_{DR}$, was measured as a function of the detuning energy, $E_d$, defined as the electron energy in the ion frame not including the electron thermal spread. The background contribution, originating from the interaction of the ion beam with residual gas in the ring, was corrected by subtracting counts until the relative difference between the trough centered at 2 eV and the peak at 10 eV was the same as that observed in the 2002 data. It is worth noting that this correction did not affect the rate coefficients at small interaction energies because of the magnitude of the DR signal in these regimes. In addition, the measured rate coefficients were corrected for the space charge of the electrons and the noncoaxial nature of the beams in the toroidal regions of the electron cooler.[17,18]

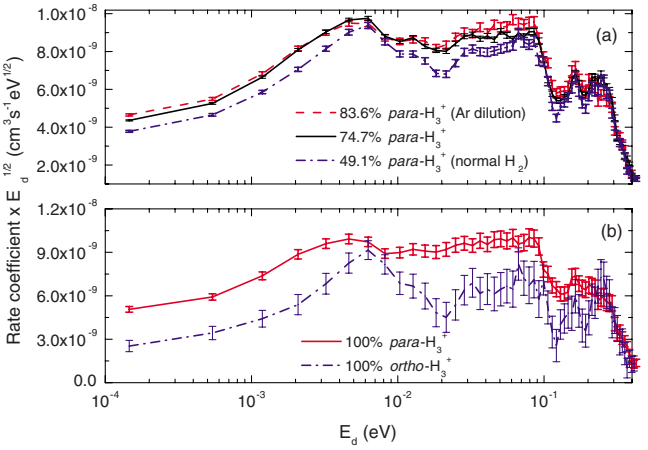


FIG. 1. (Color online) (a) Comparison of the DR rate coefficients for different para-$H_3^+$ fractions. Log scaling is avoided by applying the $E_d^{1/2}$ factor. (b) Extrapolated rate coefficients for pure ortho- and para-$H_3^+$. Uncertainties are statistical.

We performed three experiments using three different sample gases. The first experiment used the 1% dilution of enriched para-$H_2$ in argon. The second experiment was run with normal $H_2$ gas in order to compare the performance of both the supersonic expansion source and the storage ring with the results from Ref. 6. The final experimental measurements were taken using the enriched para-$H_2$ with no argon dilution. The respective ion currents after acceleration were 8.16, 54, and 48 nA.

The results of these three runs are presented in Fig. 1(a). We do not include systematic uncertainty (~16%) in our analysis because it did not change from experiment to experiment, and our focus is on the differences between the measurements. It is evident that the DR rate coefficient has a dependence on the spin modification of $H_3^+$. We observed the enriched para-$H_3^+$ produced from 97% para-$H_2$ to have a higher rate coefficient than that of the normal-$H_2$ at small $E_d$. The differences continue up to ~100 meV, with a region of much smaller differences centered around 6 meV. The measurement using argon-diluted para-$H_2$, with a para-$H_3^+$ fraction of ~83.6%, shows a slight increase over that of the undiluted para-$H_2$ sample. Figure 1(b) shows the extrapolated rate coefficients for hypothetical pure ortho- and para-$H_3^+$ derived using the 83.6% and 49.1% para-$H_3^+$ results. The same extrapolated rate coefficients can be derived using the data from the 74.7% para-$H_3^+$ experiment.

The 2007 rate coefficients for normal hydrogen were larger for all $E_d$ than observed in the 2002 data, which might be due to inaccuracies in the ion current measurement during our experiment. Great care was taken in making the ring current measurements for the 2002 run. Consequently, we multiplied our data by a normalization factor of 0.65 which was based on a comparison of the 10 eV peak heights of the 2007 and 2002 experiments. Our objective was to observe relative differences in the DR rate between para-enriched $H_3^+$ and less enriched para-$H_3^+$ samples; therefore, the consistent

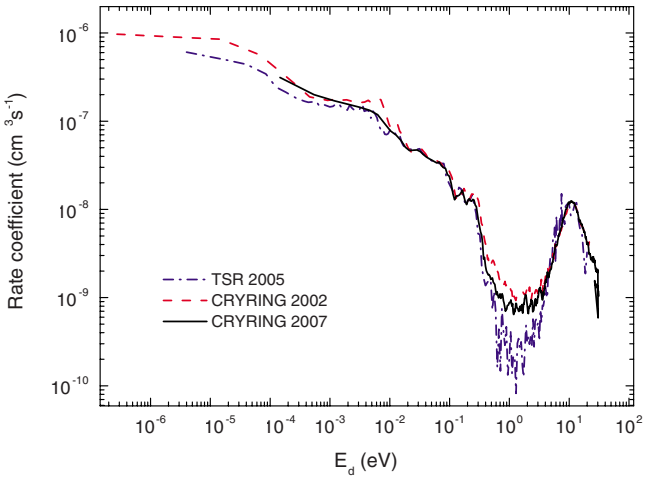


FIG. 2. (Color online) Comparison of the normal $H_2$-fed $H_3^+$ DR rate coefficients using the supersonic expansion source in 2007 and 2002; both experiments were performed with a transverse electron thermal spread ($kT_{e\perp}$) of 2 meV. Also included is a spectrum from TSR using the thermal cathode electron target with $kT_{e\perp}=4$ meV (Ref. 9). Uncertainty bars are removed to facilitate comparison of 2002 and 2007 spectra.

application of a multiplication factor to all of our data does not detract from our conclusions. A comparison with past experiments is presented in Fig. 2, and most structures above $10^{-2}$ eV are in good agreement.[6,9]

The 2007 spectrum is structurally smoother below $10^{-2}$ eV compared with the 2002 data. The rate coefficient curve at low electron energy could show less structure due to the presence of rotationally hotter ions. The indirect DR mechanism, proceeding through intermediate Rydberg states, gives rise to resonant structure in the rate coefficient. An increase in the population of excited rotational states will increase the number of resonances, resulting in a smoother curve.[10]

Our supersonic expansion source produced ions with $T_{\rm rot}\sim 60-100$ K based on the spectroscopic characterization, which was slightly higher than the value of 20–60 K obtained with the same source in 2002. Perhaps this higher $T_{\rm rot}$, combined with heating due to interactions with residual neutral molecules in the ring, led to the observed lack of structure in the cross section. That being said, experiments at TSR demonstrated that residual gas heating does not raise $T_{\rm rot}$ by more than 100–200 K.[19] It is important to note that although some excited rotational states may have contributed to our measurement, these states retain the para- to ortho-$H_3^+$ distribution as measured spectroscopically; therefore, the comparison between DR reaction rate coefficients remains valid. Para-$H_3^+$ cannot be converted to ortho-$H_3^+$ by reactive collisions in the ring, as the only likely spin-changing reaction with residual $H_2$ molecules at these high collision energies is a proton hop. Any $H_3^+$ ions formed by this process would not be at an energy that could circulate in the ring and contribute to the measurement. Additionally, we determined that the uneven depletion of spin modifications due to the different rate coefficients would not significantly affect the ortho/para ratio over our storage timescales.

The thermal rate coefficients, $\alpha(T_e)$, were calculated by integrating the energy dependent DR cross section over a Maxwellian distribution of electrons (see Ref. 6) at a given electron temperature, $T_e$. To derive the absolute cross section from the measured rate coefficient, the deconvolution procedure described in Ref. 20 was used. Table I presents the values of $\alpha(T_e)$, normalized as described above. The thermal rate coefficient at 300 K for normal $H_2$ (49.1% para-$H_3^+$) of the current experiment is in excellent agreement with that of 2002; however, the higher $T_{\rm rot}$ described earlier likely resulted in less agreement at lower electron temperatures [Fig. 3(a)]. Figure 3(b) shows the extrapolated values for 100% para-$H_3^+$ and 100% ortho-$H_3^+$. The ratio of these rate coefficients [dashed black line in Fig. 3(b)] increases as the electron temperature decreases.

TABLE I. Thermal rate coefficients, $\alpha(T_e)$, measured in the current experiment for $T_{\rm rot}=80\pm 20$ K and $T_e=300$ K. These data are derived from the measured rate coefficients, normalized to the 2002 data by a factor of 0.65. The $\alpha(T_e)$ for $n$-$H_2$ is in good agreement with Ref. 6, $0.68\times 10^{-7}$ cm$^3$ s$^{-1}$.

| % para-$H_2$ feed | % para-$H_3^+$ [a] | $\alpha(T_e)$ ($10^{-8}$ cm$^3$ s$^{-1}$) [b] |
|---|---|---|
| ... | 0 | $5.52\pm 0.77$ [c] |
| 25.0 (normal-$H_2$) | $49.1\pm 2.4$ | $6.79\pm 0.14$ |
| $97.0\pm 0.8$ | $74.7\pm 2.1$ | $7.48\pm 0.10$ |
| $97.0\pm 0.8$ (Ar dilution) | $83.6\pm 1.9$ | $7.65\pm 0.16$ |
| ... | 100 | $8.12\pm 0.36$ [c] |

[a]Spectroscopically determined after CRYRING measurements. Reported errors are $1\sigma$.
[b]Uncertainty is statistical.
[c]Extrapolated values for pure ortho- and para-$H_3^+$.

Both the $E_d$-dependent rate coefficients and the thermal rate coefficients indicate that the DR of $H_3^+$ has a nuclear spin state dependence, with that of the para spin modification proceeding at a more rapid rate. The para-$H_3^+$ has a rate coefficient almost two times larger than ortho-$H_3^+$ at low electron temperatures, with a smaller difference ($\sim$1.5) at higher temperatures. Theory predicts differences that range from more than a factor of 10 down to unity between electron temperatures of $\sim$0 and 300 K.[10]

The relatively modest (by astrophysical standards) difference in the rate coefficients of ortho- and para-$H_3^+$ sug-

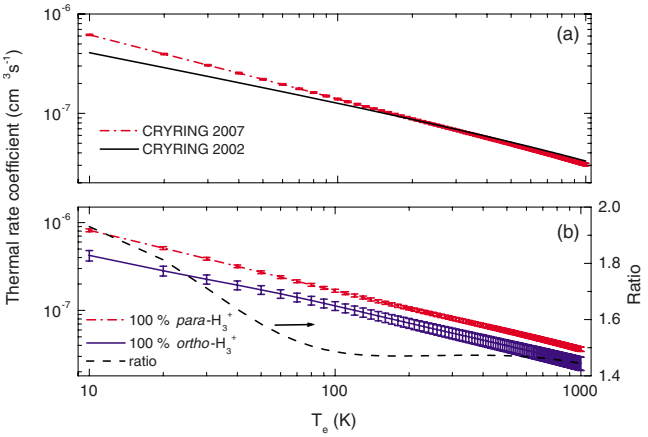


FIG. 3. (Color online) Thermal rate coefficients calculated for (a) normal $H_2$ (49.1% para-$H_3^+$) and for (b) the extrapolated 100% ortho- and para-$H_3^+$ results. Uncertainties are statistical. The dashed line represents the ratio of the thermal rate coefficients (para-$H_3^+$/ortho-$H_3^+$), with an arrow directing the reader to the appropriate axis.

gests that DR is unlikely to be the dominant process in determining the ortho:para ratio of $H_3^+$ in the diffuse interstellar medium. An even more convincing argument is the fact that para-$H_3^+$ is more abundant than ortho-$H_3^+$ in diffuse clouds;[8] yet we observe that para-$H_3^+$ has the higher DR rate coefficient. It is likely that the explanation for the interstellar ortho:para-$H_3^+$ ratio lies instead with the proton exchange reaction $H_3^+ + H_2 \rightarrow H_2 + H_3^+$. Although this reaction has a rate coefficient roughly two orders of magnitude lower than DR, the reaction partner ($H_2$) is some four orders of magnitude more abundant than electrons in diffuse clouds.

Preparations are underway to refine our supersonic expansion source design in order to consistently achieve rotationally colder ions. In addition, work is scheduled at CRYRING to minimize residual gas heating so we can better observe structural details in the DR cross section. Together, these improvements should permit a more definitive measurement of the absolute $\alpha_{DR}$ for highly enriched para-$H_3^+$.

We would like to thank the staff of the Manne Siegbahn Laboratory for valuable help during the experiment. The University of Illinois team acknowledges NSF Grant No. PHY 05-55486 for providing support, as well as a Hewlett International Travel Award. The Stockholm-based team would like to acknowledge support from the Swedish Research Council. M.K. acknowledges support from the Polish Ministry of Science and Higher Education Grant No. N202 111 31/1194, and the Swedish Institute.

[1] W. D. Watson, Astrophys. J. **183**, L17 (1973).
[2] E. Herbst and W. Klemperer, Astrophys. J. **185**, 505 (1973).
[3] T. Oka, in *Dissociative Recombination of Molecular Ions With Electrons*, edited by S. L. Guberman (Kluwer, New York, 2003), pp. 209–220.
[4] M. Larsson, Philos. Trans. R. Soc. London, Ser. A **358**, 2433 (2000).
[5] M. Larsson, B. J. McCall, and A. E. Orel, Chem. Phys. Lett. **462**, 145 (2008).
[6] B. J. McCall, A. J. Huneycutt, R. J. Saykally, N. Djuric, G. H. Dunn, J. Semaniak, O. Novotny, A. Al-Khalili, A. Ehlerding, F. Hellberg, S. Kalhori, A. Neau, R. D. Thomas, A. Paal, F. Österdahl, and M. Larsson, Phys. Rev. A **70**, 052716 (2004).
[7] V. Kokoouline and C. H. Greene, Phys. Rev. A **68**, 012703 (2003).
[8] N. Indriolo, T. R. Geballe, T. Oka, and B. J. McCall, Astrophys. J. **671**, 1736 (2007).
[9] H. Kreckel, M. Motsch, J. Mikosch, J. Glosík, R. Plašil, S. Altevogt, V. Andrianarijaona, H. Buhr, J. Hoffmann, L. Lammich, M. Lestinsky, I. Nevo, S. Novotny, D. A. Orlov, H. B. Pedersen, F. Sprenger, A. S. Terekhov, J. Toker, R. Wester, D. Gerlich, D. Schwalm, A. Wolf, and D. Zajfman, Phys. Rev. Lett. **95**, 263201 (2005).
[10] S. F. dos Santos, V. Kokoouline, and C. H. Greene, J. Chem. Phys. **127**, 124309 (2007).
[11] A. Petrignani, H. Kreckel, M. H. Berg, S. Altevogt, D. Bing, H. Buhr, M. Froese, J. Hoffmann, B. Jordon-Thaden, C. Krantz, M. B. Mendes, O. Novotný, S. Novotny, D. A. Orlov, S. Reinhardt, and A. Wolf, e-print arXiv:0810.0405.
[12] M. Quack, Mol. Phys. **34**, 477 (1977).
[13] T. Oka, J. Mol. Spectrosc. **228**, 635 (2004).
[14] A. Farkas, *Orthohydrogen, Parahydrogen, and Heavy Hydrogen* (Cambridge University Press, Cambridge, 1935), pp. 20–28.
[15] A. T. Stewart and G. L. Squires, J. Sci. Instrum. **32**, 26 (1955).
[16] M. Cordonnier, D. Uy, R. M. Dickson, K. E. Kerr, Y. Zhang, and T. Oka, J. Chem. Phys. **113**, 3181 (2000).
[17] D. R. DeWitt, R. Schuch, H. Gao, W. Zong, S. Asp, C. Biedermann, M. H. Chen, and N. R. Badnell, Phys. Rev. A **53**, 2327 (1996).
[18] A. Lampert, A. Wolf, D. Habs, J. Kenntner, G. Kilgus, D. Schwalm, M. S. Pindzola, and N. R. Badnell, Phys. Rev. A **53**, 1413 (1996).
[19] H. Kreckel, A. Petrignani, M. Berg, D. Bing, S. Reinhardt, S. Altevogt, H. Buhr, M. Froese, J. Hoffmann, B. Jordon-Thaden, C. Krantz, M. Lestinksy, M. Mendes, O. Novotný, S. Novotny, H. B. Pedersen, D. A. Orlov, J. Mikosch, R. Wester, R. Plašil, J. Glosík, D. Schwalm, D. Zajfman, and A. Wolf, J. Phys.: Conf. Ser. **88**, 012064 (2007).
[20] J. R. Mowat, H. Danared, G. Sundström, M. Carlson, L. H. Andersen, and L. Vejby-Christensen, M. af Ugglas, and M. Larsson, Phys. Rev. Lett. **74**, 50 (1995).

# Development and characterization of a source of rotationally cold, enriched *para*-$H_3^+$

Brian A. Tom,[1,*] Andrew A. Mills,[1] Michael B. Wiczer,[1,†] Kyle N. Crabtree,[1] and Benjamin J. McCall[1,2,‡]

[1] *Department of Chemistry, University of Illinois at Urbana-Champaign, Urbana, IL 61801*
[2] *Department of Astronomy, University of Illinois at Urbana-Champaign, Urbana, IL 61801*

(Dated: September 12, 2009)

In an effort to develop a source of $H_3^+$ that is almost entirely in a single quantum state ($J = K = 1$), we have successfully generated a plasma that is enriched to ∼83% in *para*-$H_3^+$ at a rotational temperature of 80K. This enrichment is a result of the nuclear spin selection rules at work in hydrogenic plasmas, which dictate that only *para*-$H_3^+$ will form from *para*-$H_2$, and that *para*-$H_3^+$ can be converted to *ortho*-$H_3^+$ by subsequent reaction with $H_2$. This is the first experimental study in which the $H_2$ and $H_3^+$ nuclear spin selection rules have been observed at cold temperatures. The ions were produced from a pulsed solenoid valve source, cooled by supersonic expansion, and interrogated via continuous-wave cavity ringdown spectroscopy. Details of the spectrometer setup are presented along with our experimental results.

## I. INTRODUCTION

In 1911, J.J. Thomson made the first experimental observation of the simplest polyatomic molecular ion, $H_3^+$ [1]. Within twenty years, the existence of two species of molecular hydrogen, defined by the intrinsic spins of their protons, was predicted by Heisenberg and Hund [2, 3]. Shortly thereafter, Bonhoeffer and Harteck [4] were able to experimentally prepare *para* hydrogen, in which the nuclear spins are antisymmetrically combined ($I$=0).

Hogness and Lunn [5] discovered that $H_3^+$ is the dominant species in hydrogenic plasmas, formed by

$$H_2 + H_2^+ \rightarrow H_3^+ + H \tag{1}$$

(exothermicity of ∼1.7 eV and Langevin rate constant, $k_L \sim 10^{-9}\,\mathrm{cm^3 s^{-1}}$ [6]). The relationship between the *ortho* and *para* spin modifications of molecular hydrogen and the *ortho* and *para* $H_3^+$ products, however, was not studied for another fifty years. New insight was gained when spin selection rules were derived by Quack [7] for reaction (1) and for the reaction

$$H_3^+ + H_2 \rightarrow H_2 + H_3^+. \tag{2}$$

The selection rules for reaction (1) dictate that only *para*-$H_3^+$ will form from pure *para*-$H_2$. Similarly, selection rules predict that reaction (2) can modify the nuclear spin distributions in predictable ways. The effect of these selection rules was experimentally observed by Uy *et al.* [8] and Cordonnier *et al.* [9] in hot (300-500 K) plasmas. In addition, Gerlich studied the closely related $D_3^+$ and $H_2$ system at much colder temperatures [10].

To enable the measurements of dissociative recombination described in [11], we developed a source of *para*-enriched, rotationally cold $H_3^+$ and a spectrometer to determine the rotational and spin modification distribution of the $H_3^+$ ions in the plasma. Ultimately, we were able to precisely determine the fraction of *para*-$H_3^+$ that existed in our cold plasma. To do this we built and used a spectrometer consisting of a difference frequency generation laser capable of probing transitions from the lowest $H_3^+$ states, $R(1,1)^u$, $R(1,0)$, and $R(2,2)^\ell$, via cavity ringdown spectroscopy (see Lindsay and McCall [12] for a description of the notation).

The remainder of this paper is organized as follows. Section II presents the theory and background on $H_2$ and $H_3^+$ spin modification interactions involved in the process of *para*-$H_3^+$ formation. The details of our experimental design are discussed in section III, and the results of the spectroscopic characterization of our ion source are presented in section IV.

## II. THEORY AND BACKGROUND

Quack [7] derived the selection rules that govern transitions between both rovibronic and nuclear spin states in reactive collisions involving identical nuclei. He used group theory to understand the symmetries of these internal states as they transitioned from reactant, to completely 'scrambled' reaction intermediate, to product. The nuclear spin configurations of the species in hydrogen-containing plasmas can thus be predicted.

A different, albeit equivalent, method was proposed by Oka [13]. In this method, the rovibronic states of the molecules are no longer explicitly considered, due to the fact that these states are automatically symmetrized with respect to permutation. His method focuses solely on the nuclear spin, and uses angular momentum algebra instead of group theory to calculate the spin states of the products. Both methods are successful because overall nuclear spin is essentially conserved between reactants and products (there are hyperfine interactions that prevent nuclear spin from being completely conserved, but these are insignificant due to the weak nuclear magnetic interaction [8]). Using angular momentum algebra [14],

*Present Address: Department of Chemistry, United States Air Force Academy, CO 80840
†Present Address: Department of Physics, Massachusetts Institute of Technology, Cambridge, MA 02139
‡Electronic address: bjmccall@illinois.edu

one can account for the conservation of spin using,

$$\mathcal{D}_{I_1} \otimes \mathcal{D}_{I_2} = \mathcal{D}_{I_1+I_2} \oplus \mathcal{D}_{I_1+I_2-1} \oplus \cdots \oplus \mathcal{D}_{|I_1-I_2|}. \quad (3)$$

With this formula, the weighting factors for the product spin species of reaction 1 can be derived, and are presented in Table I (see [13] for the detailed derivation). The basis of this work is the relationship presented in the last line of this table. Only the *para*-$H_3^+$ spin modification can form from *para*-$H_2$.

TABLE I: The product spin weights for $H_2$+$H_2^+$ →$H_3^+$+H. The overall weighting factor is the product of the reactant nuclear spin degeneracies.

| | | Products | |
|---|---|---|---|
| Reactants | Weight | *o*-$H_3^+$ + H | *p*-$H_3^+$ + H |
| *o*-$H_2$ + *o*-$H_2^+$ | 9 | 6 | 3 |
| *o*-$H_2$ + *p*-$H_2^+$ | 3 | 1 | 2 |
| *p*-$H_2$ + *o*-$H_2^+$ | 3 | 1 | 2 |
| *p*-$H_2$ + *p*-$H_2^+$ | 1 | 0 | 1 |

Reaction (1) may establish one particular spin modification or combination of nuclear spin modifications in the $H_3^+$ population, however, reaction (2) will occur immediately following the formation of $H_3^+$ given the abundance of neutral molecular hydrogen in hydrogenic plasmas (roughly 4 orders of magnitude more abundant than the ionic species). Changes to the spin modifications of the constitutents will undoubtedly occur. Reaction (2) happens in one of three different ways: identity (4), proton hop (5), or hydrogen exchange (6).

$$H_3^+ + \tilde{H}_2 \rightarrow H_3^+ + \tilde{H}_2 \quad (4)$$

$$H_3^+ + \tilde{H}_2 \rightarrow H\tilde{H}_2^+ + H_2 \quad (5)$$

$$H_3^+ + \tilde{H}_2 \rightarrow H_2\tilde{H}^+ + H\tilde{H} \quad (6)$$

The hydrogens originally in the $H_2$ reactant are designated as $\tilde{H}$ in order to illustrate the differences between the three reactions. The $H_3^+$ spin branching ratios for reactions (4,5,6), the detailed derivation of which are also found in [13], are listed in Table II.

In the context of producing a hydrogenic plasma that is highly enriched in *para*-$H_3^+$, it is necessary to understand the effects of these three reactions on the conversion of *para*-$H_3^+$ to *ortho*-$H_3^+$. Upon inspection of Table II, there is clearly no $H_3^+$ spin conversion in the identity reaction (4). If *para*-$H_3^+$ combines with *para*-$H_2$ in the proton hop reaction (5), the product $H_3^+$ also emerges without spin conversion. This makes the exchange reaction the dominant $H_3^+$ spin conversion mechanism in a plasma formed from pure *para*-$H_2$.

The underlying assumption in these models for nuclear spin conversion is that the product states will be formed from combinations of reactant states according only to the statistical constraints imposed by the conservation of nuclear spin. This assumption is valid at higher temperatures where there is sufficient energy for certain allowed, but thermodynamically unfavorable reactions to occur. For example, reactions in which *para*-$H_2$ is converted to *ortho*-$H_2$ are allowed by spin-conservation in some cases, but are endothermic by at least 118.5 $cm^{-1}$. At low temperatures, this statistical treatment is thus incomplete, however, this limitation is not addressed in this work.

TABLE II: $H_3^+$ spin modification ratios in the reaction $H_3^+ + H_2 \rightarrow H_3^+ + H_2$. When the reactants consist of pure *para* $H_3^+$ and $H_2$, the only mechanism leading to *ortho*-$H_3^+$ is the exchange reaction (6).

| Reactant Spin Modifications and Reaction Mechanisms | | Product Fractions *ortho*-$H_3^+$ | *para*-$H_3^+$ |
|---|---|---|---|
| *ortho*-$H_3^+$+*ortho*-$H_2$ | | | |
| Identity | → | 1 | 0 |
| Proton Hop | → | 2/3 | 1/3 |
| Hydrogen Exchange | → | 2/3 | 1/3 |
| *ortho*-$H_3^+$+*para*-$H_2$ | | | |
| Identity | → | 1 | 0 |
| Proton Hop | → | 0 | 1 |
| Hydrogen Exchange | → | 2/3 | 1/3 |
| *para*-$H_3^+$+*ortho*-$H_2$ | | | |
| Identity | → | 0 | 1 |
| Proton Hop | → | 2/3 | 1/3 |
| Hydrogen Exchange | → | 1/3 | 2/3 |
| *para*-$H_3^+$+*para*-$H_2$ | | | |
| Identity | → | 0 | 1 |
| Proton Hop | → | 0 | 1 |
| Hydrogen Exchange | → | 1/3 | 2/3 |

For the present experimental purposes, we were primarily concerned with producing a highly enriched *para*-$H_3^+$ plasma. We therefore explored ways to minimize the effects from reactions (5) and (6) in order to realize the highest possible *para*-$H_3^+$ enrichment.

## III. EXPERIMENT

The experimental setup consisted of a *para*-$H_2$ converter and system for testing the level of enrichment, a mid-IR difference frequency generation laser integrated into a continuous wave cavity ringdown spectrometer, a pulsed discharge supersonic expansion source, and the software necessary to synchronize the ringdown events with the source. Each of these aspects of our experiment will be discussed below.

### A. Parahydrogen generation and enrichment testing

A system was designed and built to reliably generate highly enriched *para*-$H_2$ (∼99.99%). The apparatus consisted of a hydrogen generator (Parker Hannafin H2-1200) coupled to a closed-cycle $^4$He cryostat (Janis CCS-100/204 Optical 10K Refrigerator). The cryostat was modified with a gas line and cold head section that was filled with a paramagnetic catalyst. We also developed a technique to measure the enrichment of the *para*-$H_2$ using nuclear magnetic resonance, and we built a device to do the same using thermal conductance [15]. Additional details regarding these systems are presented in [16].

### B. Difference frequency generation laser

The mid-infrared region contains the fundamental rovibrational absorptions for many species. Continuous wave (CW) light sources provide a desirable level of frequency stability for high-resolution spectroscopy. Many tunable cw sources in this region, such as quantum cascade lasers, color-center lasers, and lead salt diode lasers suffer from practical drawbacks, such as cryogenic cooling, narrow tunability, and incomplete wavelength coverage (due to mode hops) [17].

Difference-frequency generation (DFG) can produce widely-tunable, mid-IR light at the difference frequency of two pump lasers that have been mixed in a nonlinear optical crystal. Pine first demonstrated the collection of high-resolution spectra using DFG as a light source in 1974 [18]. DFG also offers narrow linewidth and high spectral resolution [19].

The intensity of the difference-frequency light can be increased using crystals that are phase matched for the pump lasers [20]. Periodically poled crystals achieve this via a process called quasi-phase matching, which leads to amplification of the difference frequency output [21]. Pump lasers are chosen to give the desired wavelength. In order to produce light between 2.8 and 4.8 microns, we have constructed a DFG laser using Ti:Sapph and Nd:YAG CW lasers that are mixed in a periodically poled lithium niobate (PPLN) crystal, similar to the lasers built by Cao *et al.*, Deng *et al.*, and Miyamoto and Momose [22–24].

The experimental setup is shown in Figure 1. A monolithic Nd:YAG (Innolight Mephisto 1000NE) laser produced CW elliptically-polarized light. Quarter and half wave plates changed the polarization to linear and vertically polarized light. An acousto-optic modulator (Brimrose TEM-85-2-1064) was used to modulate the YAG light. A Nd:$YVO_4$ laser (Spectra Physics Millenia 10s-Series) produced pump radiation at 532 nm for the Ti:Sapph ring laser (Sirah Matisse TS). The YAG and Ti:Sapph laser beams were made collinear with a dichroic beam combiner. An anti-reflection coated 20 cm achromat doublet focused both lasers into the periodically

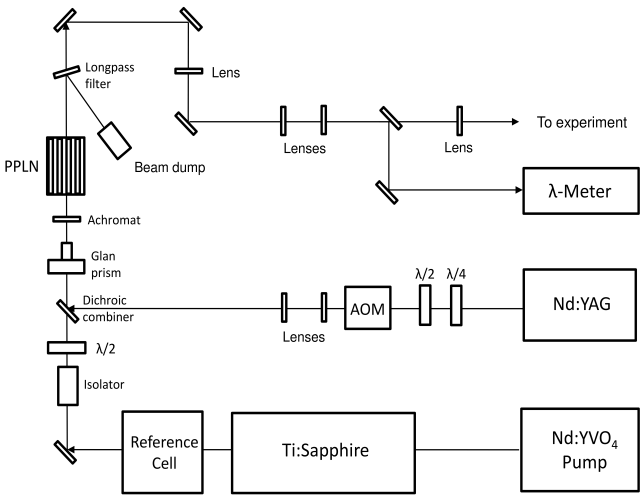


FIG. 1: DFG System

poled lithium niobate PPLN crystal (Stratophase DFG2-40) whose temperature was fixed via an oven (Thorlabs OV40) and temperature controller (Thorlabs TC200). The lasers were focused with near unity (0.9) confocal parameters (3.6 cm Ti:Sapph, 4 cm YAG). Several $CaF_2$ lenses were used to collimate the IR light and match the beam waist to the size of a cavity used for ringdown [25]. A long pass filter (Infrared Optical LP-2500-F) was used to dump the pump lasers, and a $BaF_2$ window diverted some of the IR light into a 30 MHz precision wavemeter (Bristol 621A-IR), which enabled us to tune the laser to the starting point for each scan. A ringdown cavity was formed using two plano-concave (6m radius of curvature) mirrors that are highly reflective (99.98%) at 4 microns (Los Gatos 901-0008-4000). These mirrors formed the optical cavity for ringdown, and they also served as the windows for our vacuum system. The length of the cavity (∼0.75 m) was dithered in order to achieve resonance with the incident mid-IR light using a piezoelectric-transducer (Piezomechanik HPSt 150/20-15/12 VS 35). The light leaking out of the ringdown cavity was focused onto a 1 mm diameter indium antimonide photovoltaic detector (Infrared Associates InSb 1000), whose voltage output was amplified with a preamplifier (Infrared Systems Development), with a bandwidth from 500 Hz to 1 MHz.

As the index of refraction of the nonlinear crystal is a function of both wavelength and temperature, it is necessary to determine an operating temperature for the crystal in order to produce light at various wavelengths. By using the phase mismatch condition (Equation 2 from Jundt [26] and the equation for the index of refraction found in Deng *et al.* [27]), a phase matching curve was constructed for our PPLN crystal and pump lasers. The predicted temperatures for wavelengths accessed in this work were found to be within 2 degrees of those predicted by Deng *et al.* [27].

### C. Pulsed discharge supersonic expansion source

The pulsed source was originally designed for an earlier $H_3^+$ dissociative recombination experiment [28]. It consisted of a solenoid valve (General Valve Series 9) which modulated the gas flow by extracting a teflon poppet from a 500 $\mu$m pinhole. The gas expanded through a ring electrode, then continued downstream through a skimmer approximately 4.2 cm away. The solenoid was controlled using a locally-built driver box which in turn was charged with an external power supply, and triggered by a digital delay generator (Quantum Composers 9518+). A separate high voltage power supply provided potential for the discharge electrode via another locally-built driver box, which was triggered by the same digital delay generator.

A TTL pulse of approximately 100 $\mu$s was sent to the source driver box in which a set of six, 22 $\mu$F (450 V) capacitors would discharge 300V to drive the source. Although the TTL pulse was 100 $\mu$s in length, the gas pulse was typically 0.75-1.0 ms in duration due to the mechanical response of the solenoid. The solenoid (gas) pulse was imbedded in a 2 ms discharge pulse. The discharge potential was between -450-800 V, which was optimal for producing enough ions for spectroscopy while minimizing arcing. Neither the temperature of the expansion nor the *para*-$H_3^+$ fraction showed a dependence on the discharge voltage setting. The gas pulse was initiated 200-500 $\mu$s after the electrode was charged.

The expansion was backed by 2 atm of n-$H_2$ (normal $H_2$ where *ortho:para*=3:1), 99.9%-enriched *para*-$H_2$, or enriched *para*-$H_2$ diluted in argon. This pressure was at a high enough differential with respect to the chamber pressure for collisional cooling to occur in the Campargue-type expansion [29]. The chamber itself was locally designed and built, and was evacuated with a two stage Roots blower (Leybold RA-13000 and WS-2001) with rotary vane backing pump (Leybold SV-630) capable of 3500 L $s^{-1}$ pumping speed. The laser beam probed the plasma approximately 3.8 cm downstream from the source pinhole, which was 8.3 cm upstream of the calculated position of the Mach disk.

### D. Pulsed ringdown integration code

The integration of continuous wave cavity ringdown with our pulsed source provided an interesting challenge. As described in §III-B, and in Widicus Weaver *et al.* [30], one of the cavity mirrors was dithered by a piezo actuator. This caused the cavity to periodically move in and out of resonance with the incident light. Spectroscopy is relatively straightforward when the test gas is continuously present, but a pulsed source requires anticipation of the ringdown event, as discussed in Birza *et al.* [31].

To account for this, we integrated a ringdown prediction code with our LabWindows data acquisition routine. The ringdown data and the piezo ramp voltage (a sawtooth function) were fed to the computer via a 14-bit digitizer (National Instruments 5122). The sawtooth function was analyzed to determine peak and minimum voltage, as well as the frequency of the sweep.

Up to two ringdown events were recorded per upsweep of the sawtooth along with the voltage at which the ringdowns occurred. After approximately 3 ms of exponential fitting of the ringdown decay and other calculations, another measurement was taken to determine the sign of the slope of the piezo sweep. This was done to ensure the measurements were only being taken on the upsweeps of the piezo ramp. If a ringdown event was detected at the same voltage on the next piezo upsweep, the ringdown was considered repeatable. This trigger voltage was then offset to a lower voltage than measured. This 'lead' voltage was calculated from $dV/dt$, which was derived from the measured sawtooth frequency and a lead time which could be set by the operator in $\mu$s. The intent of the lead voltage was to account for valve actuation and ion time of flight so the heart of the discharge pulse would be in the laser beam path at the time of the ringdown (Figure 2).

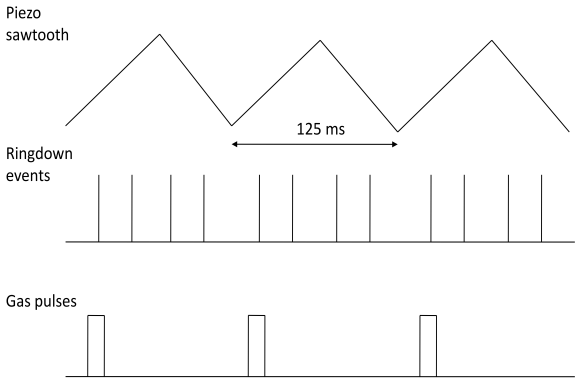


FIG. 2: Gas pulses were synchronized with ringdown events, which occured periodically with the dithering of one of the ringdown mirrors (adapted from [31]).

If a ringdown was observed when the source had been triggered, then the absorbance data from that ringdown event was recorded in an array of 'sample' events. The majority of ringdown events, however, were deemed unrepeatable by the prediction code. The absorbances from these events were recorded in a 'baseline' array. The average of the baseline spectra was subtracted from the average of the sample spectra in order to calculate the final absorbance spectrum. In order to reduce the influence of time constants that resulted from higher-order transverse modes of the cavity, the ringdown code only stored points that were among the 50% closest to the mean (box and whiskers), as described in [30]. Additional logic was added to reject data if the predicted and actual ringdown events occurred outside of an operator-set time tolerance, and ringdowns that occurred too close

to the peak of the piezo sweep were rejected in order to prevent measurements on the down-sweep.

A trigger circuit was designed to allow the software to interface with the pulse generator. The prediction code sent an output voltage to a homebuilt op-amp switch. The voltage was held at a low value as long as there were no predicted ringdowns. The op amp switch was also fed with the same piezo sawtooth voltage as was sent to the prediction code. If a repeatable ringdown was detected, the output voltage was set to the calculated lead voltage and the op-amp would trigger as soon as it detected equivalence between the two voltages (this circuit is depicted in Figure 3). An additional op-amp

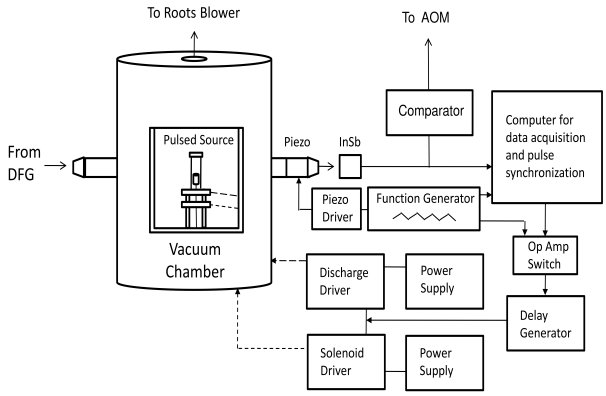


FIG. 3: The ringdown/pulsed source experimental setup.

was included in the circuit as a Schmitt trigger in order to sharpen the output TTL signal that was sent to the digital delay generator.

For this experiment, the piezo was dithered with a frequency of 8 Hz (∼3 ringdown events per period). Typically, 20-30 total ringdown events were acquired per second, approximately 5 of which occurred with sample present. The baseline RMS of the background spectrum was $1 \times 10^{-8}$ cm$^{-1}$, and the baseline RMS of the spectrum with $H_3^+$ present was $8 \times 10^{-9}$ cm$^{-1}$. The RMS for the spectrum with sample present was consistently lower despite having fewer data points. This was because the ringdown events with sample present were by definition repeatable over several piezo periods and were the result of the stronger, more consistent $TEM_{00}$ resonances. Furthermore, the ringdown decays that were counted towards background but were less intense and less repeatable tended to have lower time constants because they were likely the product of more quickly decaying transverse modes. This skewed the background spectra to higher absorption by approximately $5 \times 10^{-9}$ cm$^{-1}$ and caused the baseline of the background-subtracted spectra to be negative by the same amount.

The DFG was scanned by tuning the Ti:Sapph laser. Voltage commands were sent from the ringdown code to the Ti:Sapph laser by way of virtual interface storage architecture (VISA). Forty ringdown samples were taken at each point, after which the ringdown code would step the laser by ∼50 MHz.

Although the code successfully predicted the ringdown events, the measurements varied in such a way as to lead to significant (factor of two to three) differences in the lineshape or the calculated peak height, even after averaging over forty samples. There were multiple causes of this variation, such as arcing and pulse timing jitter. Arcing arose from deposits on the electrode as well as inhomogeneity in the gas pulses. With regards to timing jitter, if the resonance was slightly earlier or later than predicted, the measurement would occur in different locations along the gas pulse. There were also long-term effects which may have been due to the flushing of impurities through the gas feed line. Both the short- and long-term variations were mitigated by normalizing and fitting the data. We normalized using a boxcar integrator (Stanford Research SR250) to record an average discharge current during the measurements. The spectra were then divided by this current. In addition, each peak was fit with a Gaussian lineshape, and it was the peak height of this Gaussian that was measured and recorded. The effectiveness of these techniques was evident from the shrinking standard deviation that occurred with their application.

## IV. OBSERVED RESULTS

Our experimental measurements had the following three objectives: 1) to determine the rotational temperature of the expansion; 2) to measure the *para*-$H_3^+$ enrichment that resulted from using highly enriched *para*-$H_2$; and 3) to observe the effect of dilution in an inert carrier gas on the fraction of *para*-$H_3^+$ in the expansion.

### A. Temperature measurements

We measured the temperature of the expansion by comparing the relative abundances of the *para* and *ortho* spin modifications of $H_3^+$ formed from a normal-$H_2$ precursor gas (where *ortho:para*=3:1). This so-called excitation temperature ($T_{ex}$) has often been used as a proxy for the rotational temperature ($T_{rot}$) [28, 32, 33]. The excitation temperature can be calculated using the equation,

$$\frac{N_{(1,0)}}{N_{(1,1)}} = \frac{g_{(1,0)}}{g_{(1,1)}} e^{-\Delta E_{1,0-1,1}/k_B T_{ex}}, \tag{7}$$

where the ratio of nuclear spin degeneracy $g_{(1,0)}/g_{(1,1)} = 4/2 = 2$, and the value for $\Delta E_{1,0-1,1} = 22.84$ cm$^{-1}$ [12]. In place of $N_{(1,0)}$ and $N_{(1,1)}$, we used the normalized peak absorbances of the rovibrational transitions $R(1,0)$ and $R(1,1)^u$ for *ortho* and *para*-$H_3^+$ respectively, divided by the squares of their transition dipole moments, $\mu^2_{R(1,0)} = 0.0259$ D$^2$ and $\mu^2_{R(1,1)^u} = 0.0158$ D$^2$. These transitions

are separated by only 0.32 $cm^{-1}$, which made it easy to measure the peaks in quick succession.

In some instances, we measured rotational temperature directly by comparing the *para*-$H_3^+$ $R(1,1)^u$ and $R(2,2)^\ell$ transitions. In all cases we found a good correlation between the excitation and rotational temperatures.

The temperature of the expansion was sensitive to the condition of the poppet, as also observed in [28], as well as how tightly the poppet was seated in the source pinhole. Our probe region was approximately 3.8 cm downstream of the electrode, and about 4 mm in front of a skimmer. We took measurements of the temperature throughout the experiment. If the temperature was too hot (>100 K), we would 'tune' or replace the poppet before proceeding. As can be seen from Table III, the typical temperature in our expansion was between 60-100 K, and the variations were likely due to the changing conditions of the poppet.

TABLE III: Excitation and rotational temperatures measured using normal and *para*-$H_2$. The 'a' and 'b' designations identify temperatures measured in close succession. The absorbance values are given in $10^{-6}$ $cm^{-1}$.

| | | Absorbance | | | Temperature (K) | |
|---|---|---|---|---|---|---|
| | Feed gas | $R(1,1)^u$ | R(1,0) | $R(2,2)^\ell$ | $T_{ex}$ | $T_{rot}$ |
| 1 | normal-$H_2$ | 0.35 | 0.84 | - | 98 | - |
| 2 | para-$H_2$ | 0.41 | - | 0.07 | - | 61 |
| 3a | normal-$H_2$ | 1.32 | 2.83 | - | 77 | - |
| 3b | normal-$H_2$ | 1.32 | - | 0.43 | - | 79 |
| 4 | normal-$H_2$ | 0.25 | 0.56 | - | 90 | - |
| 5a | normal-$H_2$ | 0.98 | 2.1 | - | 76 | - |
| 5b | normal-$H_2$ | 0.98 | - | 0.28 | - | 75 |

It is unclear why we did not observe temperatures colder than 60-100 K in our expansion. This same source produced ions at $T_{ex}$ = 20-60 K a few years earlier [28]. One possible cause was the gas-pulse/discharge-pulse sequencing. In the present experiment we embedded the gas pulse in a longer voltage pulse, which could have resulted in additional heating.

### B. *Para*-$H_3^+$ fraction in undiluted $H_2$ samples

The intensities of the $R(1,0)$ *ortho*-$H_3^+$ and the $R(1,1)^u$ *para*-$H_3^+$ peaks were measured for normal and highly enriched (99.99%) *para*-$H_2$ precursor gases. The purpose of these measurements was to quantitatively characterize the dependence of the *para*-$H_3^+$ fraction in the plasma on the *para* enrichment of the precursor gas. The simple equation,

$$\%\ para\text{-}H_3^+ = \frac{\Sigma\, N_{para}}{\Sigma\, N_{para} + \Sigma\, N_{ortho}}, \qquad (8)$$

was used to derive the *para*-$H_3^+$ percentage, where the $\Sigma N$ values were calculated using the measured intensities of the *para*- and *ortho*-$H_3^+$ ground state transitions. To go from the ground state intensities to the various $\Sigma N$, it was assumed that the rotational states within the *para* and *ortho* manifolds were thermally populated. Boltzmann distributions were applied assuming $T_{rot} = 80 \pm 20$K (based on the temperature measurements described in the previous section). At 80 K, almost 25% of *para*-$H_3^+$ ions are in rotationally excited states whereas only 4% of *ortho*-$H_3^+$ are excited out of the ground state.

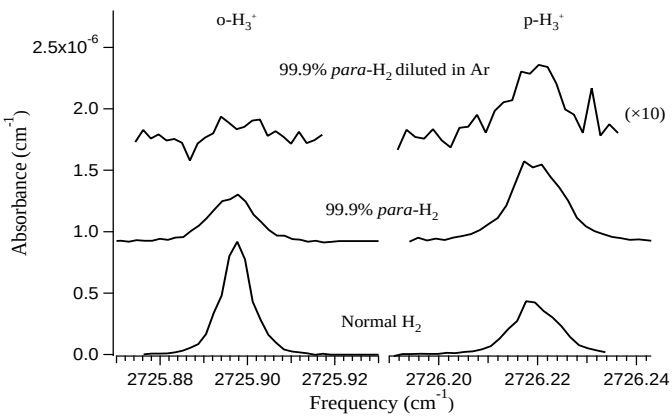


FIG. 4: Comparison of spectra for $H_3^+$ for various precursor gases. Increasing the *para*-$H_2$ enrichment of the feed gas resulted in a higher enrichment of *para*-$H_3^+$. The plots are shifted vertically for clarity.

Using a highly enriched sample of *para*-$H_2$ in the discharge resulted in a plasma with $\sim 78.5 \pm 2.2\%$ *para*-$H_3^+$. Figure 4 depicts the changes in peak heights of $R(1,0)$ and $R(1,1)^u$ as the enrichment of the *para*-$H_2$ precursor gas was increased from that of normal-$H_2$ to 99.99%. These results are evidence that the selection rules as described in §II are at work at the cold, astrophysically relevant temperatures of a supersonic expansion. The shift in intensity from *ortho*- to *para*-$H_3^+$ with the increase in *para*-$H_2$ feed gas enrichment validates the prediction that *para*-$H_3^+$ is the dominant spin species formed in highly enriched *para*-$H_2$ plasmas.

### C. *Para*-$H_2$ dilution in inert gas

Measurements were taken using dilutions of various enrichments of *para*-$H_2$. Dilution in a non-hydrogenic gas reduces the number of reactions between the *para*-$H_3^+$ ions and $H_2$. The rate of reaction (2) for a given $H_3^+$ goes as $k\cdot[H_2]$, where $k$ is the rate constant and $[H_2]$ is the number density of $H_2$. If the overall number of molecules in the expansion remains the same, but $[H_2]$ is reduced by dilution in an inert gas, then the number of $H_3^+$ to $H_2$ interactions will decrease. Thus, dilution will reduce the deleterious effect of the exchange reaction (6) on the *para*-$H_3^+$ enrichment of the plasma. As was shown in §II, the exchange is the primary mechanism by which *para*-$H_3^+$ is converted to *ortho*-$H_3^+$ in *para*-enriched plasmas.

TABLE IV: The *para*-$H_3^+$ fraction observed with two different *para*-$H_2$ enrichments, including argon dilution results for the higher enrichment. A Boltzmann distribution for $T_{rot} = 80$ K has been applied.

| Starting *para*-$H_2$ (%) | Percent $H_2$ [a] | *para*-$H_3^+$ (%) [b] |
|---|---|---|
| 25 | 100 | 49.1 ± 2.4 |
| 99.99 | 100 | 78.5 ± 2.2 |
| | 15 | 78.0 ± 1.8 |
| | 5 | 70.9 ± 2.2 |
| | 0.8 | 83.3 ± 1.8 |

[a]The dilution was carried out using pressure $\left(\frac{P_{H_2}}{P_{H_2}+P_{Ar}}\right)$

[b]The reported errors are $1\sigma$, and are calculated from the standard deviation of multiple measurements at a particular point and a temperature uncertainty of ±20 K.

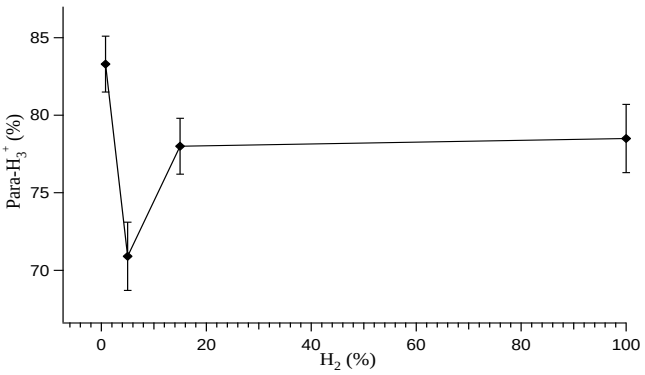


FIG. 5: The *para*-$H_3^+$ fraction versus argon dilution for 99.99% *para*-$H_2$. Uncertainties are 1 $\sigma$.

The dilutions were carried out by pre-mixing the desired pressures of $H_2$ and argon or neon in order to provide 2 atm of backing pressure for the source. In all cases, the $H_3^+$ signal was attenuated by dilution as can be seen in Figure 4. The data are presented in Table IV. Not surprisingly, the results of the dilution experiments, graphically depicted in Figure 5, show that the *para*-$H_3^+$ fraction has a dependence on the extent of the dilution.

In every experiment where the hydrogen feed gas was diluted in argon, we observed a one or two order of magnitude decrease in the number density of $H_3^+$ ions produced. When the hydrogen was diluted between 5-15% in argon, there was an unexpected decrease in the fraction of [*para*-$H_3^+$]/[*total*-$H_3^+$] in the plasma. The reason for this decrease is not understood at present, but could have an impact on Ar-$H_3^+$ action spectroscopy schemes as employed in [34–36]. Despite this, we observed an increase in the *para*-$H_3^+$ fraction when the $H_2$ was diluted to ∼1% in argon.

We attempted to measure the *para*-$H_3^+$ fraction in a neon carrier gas. The 10% dilutions in neon resulted in a signal similar to that of the 15% dilution in argon, however, when a ∼1% dilution was analyzed, the $H_3^+$ signal was almost completely quenched.

## V. CONCLUSIONS

The manifestation of $H_2$ and $H_3^+$ nuclear spin selection rules in a plasma generated using a pulsed supersonic expansion have resulted in a source of highly enriched, rotationally cold, *para*-$H_3^+$. We have achieved an 83.3% enrichment by diluting 99.9% *para*-$H_2$ in argon to 1% by pressure. We have also observed unexpected behaviors at intermediate argon dilutions. These behaviors warrant further investigation, perhaps by simultaneous laser and mass spectroscopic measurements. This source can be used for reaction dynamics experiments between $H_2$ and $H_3^+$, along with experiments that measure properties of *para*-$H_3^+$ enriched plasmas at astrophysically relevant temperatures.

Future work includes the development of a more reliable source that can consistently produce rotationally-cold ions. As described in §IV A, the temperature conditions of the expansion varied depending on the tuning and condition of the source poppet. A piezo valve has been shown to produce a colder plasma over a longer period of time [37]. Such a source should be capable of achieving expansion temperatures that are 40-50 K lower than those measured in the present work.

## VI. ACKNOWLEDGMENTS

We would like to thank Takeshi Oka for valuable discussions on the dynamics of the hop and exchange reactions, Dana Dlott for the loan of equipment, and Dr. Jim Wentz for assistance in building many of the electronic devices used in this experiment. In addition, we thank Nicole Tom for her work on the DFG schematic. This research was funded by the National Science Foundation AMO Physics grant PHY-0555486.

[1] J. J. Thomson, Phil. Mag. **21**, 225 (1911).
[2] W. Heisenberg. Z. f. Physik **41**, 239 (1927).
[3] F. Hund, Z. f. Physik **42**, 93 (1927).
[4] K. F. Bonhoeffer and P. Harteck, Z. Phys. Chem. **B4**, 113 (1929).
[5] T. R. Hogness and E. G. Lunn, Phys. Rev., **26**, 44 (1925).
[6] T. Oka, Rev. Mod. Phys., **64**, 1141 (1992).
[7] M. Quack, Mol. Phys., **34**, 477 (1977).
[8] D. Uy, M. Cordonnier, and T. Oka, Phys. Rev. Lett., **78**, 3844 (1997).
[9] M. Cordonnier, D. Uy, R. M. Dickson, K. E. Kerr, Y. Zhang, and T. Oka, J. Chem. Phys., **113**, 3181 (2000).

[10] D. Gerlich, J. Chem. Soc. Faraday Trans., **89**, 2199 (1993).
[11] B. A. Tom, V. Zhaunerchyk, M. B. Wiczer, A. A. Mills, K. N. Crabtree, M. Kaminska, W. D. Geppert, M. Hamberg, M. af Ugglas, E. Vigren, W. J. van der Zande, M. Larsson, R. D. Thomas, and B. J. McCall, J. Chem. Phys., **130**, 031101 (2009).
[12] C. M. Lindsay and B. J. McCall, J. Mol. Spec., **210**, 60 (2001).
[13] T. Oka, J. Mol. Spec., **228**, 635 (2004).
[14] L. D. Landau and E. M. Lifshitz, *Quantum Mechanics*, Pergamon Press (1977).
[15] A. Farkas,*Orthohydrogen, Parahydrogen, and Heavy Hydrogen*, Cambridge Univ. Press (1935).
[16] B. A. Tom, Y. Miyamoto, S. Bhasker, T. Momose, and B. J. McCall, Rev. Sci. Inst., **80**, 016108 (2009).
[17] U. Simon, C. E. Miller, C. C. Bradley, R. G. Hulet, R. F. Curl, and F. K. Tittel, Optics Lett., **18**, 1062 (1993).
[18] A. S. Pine, J. Opt. Soc. America. V. 64, **12**, 1683 (1974).
[19] W. Chen, G. Mouret, J. Burie, and D. Boucher, Int. J. of Infrared and Millmeter Waves, **19**, 409 (1998).
[20] U. Simon, Z. Benko, M. W. Sigrist, R. F. Curl, and F. K. Tittel, Applied Optics, **32**, 6650 (1993).
[21] K. W. Aniolek, P. E. Powers, T. J. Kulp, B. A. Richman, and S. E. Bisson, Chem. Phys. Lett. **302**, 555 (1999).
[22] Z. Cao, X. Gao, L. Deng, W. D. Chen, Y. Yuan, W. Zhang, and Z. Gong, Spectrochim. Acta Part A., **68**, 74 (2006).
[23] L. Deng, L. Han, W. Liang, Z. Cao, C. Xu, W. Zhang, Z. Gong, and X. Gao, Optics and Lasers in Engineering, **45**, 1055 (2007).
[24] Y. Miyamoto and T. Momose, to be submitted.
[25] D. Romanini, A. A. Kachanov, N. Sadeghi, and F. Stoeckel, Chem. Phys. Lett. **264**, 316 (1997).
[26] D. H. Jundt, Opt. Lett., **22**, 1553 (1997).
[27] L. H. Deng, S. M. Gao, Z. S. Cao, W. D. Chen, Y. Q. Yuan, W. J. Zhang, and Z. B. Gong, Optics Communications, **268**, 110 (2006).
[28] B. J. McCall, A. J. Huneycutt, R. J. Saykally, N. Djuric, G. H. Dunn, J. Semaniak, O. Novotny, A. Al-Khalili, A. Ehlerding, F. Hellberg, S. Kalhori, A. Neau, R. D. Thomas, A. Paal, F. Österdahl, and M. Larsson, Phys. Rev. A, **70**, 052716 (2004).
[29] R. Campargue, J. Phys. Chem., **88**, 4466 (1984).
[30] S. L. Widicus Weaver, M. B. Wiczer, B. Negru, J. P. DiGangi, B. A. Tom, and B. J. McCall, J. Mol. Spec., **249**, 14 (2008).
[31] P. Birza, T. Motylewski, D. Khoroshev, A. Chirokolava, H. Linnartz, and J.P. Maier, Chem. Phys., **283**, 119 (2002).
[32] T. Oka, PNAS, **103**, 12235 (2006).
[33] N. Indriolo, T. R. Geballe, T. Oka, and B. J. McCall, Astrophys. J., **671**, 1736 (2007).
[34] H. Kreckel, A. Petrignani, M. Berg, D. Bing, S. Reinhardt, S. Altevogt, H. Buhr, M. Froese, J. Hoffmann, B. Jordon-Thaden, C. Krantz, M. Lestinksy, M. Mendes, O. Novotný, S. Novotny, H. B. Pedersen, D. A. Orlov, J. Mikosch, R. Wester, R. Plašil, J. Glosík, D. Schwalm, D. Zajfman, and A. Wolf, J. Phys.: Conf. Ser., **88**, 012064 (2007).
[35] A. Petrignani, H. Kreckel, M. H. Berg, S. Altevogt, D. Bing, H. Buhr, M. Froese, J. Hoffmann, B. Jordon-Thaden, C. Krantz, M. B. Mendes, O. Novotný, S. Novotny, D. A. Orlov, S. Reinhardt, and A. Wolf, arXiv: 0810.0405 (2008).
[36] H. Kreckel, D. Bing, S. Reinhardt, A. Petrignani, M. Berg, and A. Wolf, J. Chem. Phys., **129**, 164312 (2008).
[37] D. Proch and T. Trickl, Rev. Sci. Inst. **60**, 713 (1989).